PERGAMON

Deep-Sea Research II 45 (1998) 1961–1999

DEEP-SEA RESEARCH
PART II

Atmospheric forcing in the Arabian Sea during 1994–1995: observations and comparisons with climatology and models

R.A. Weller[a,*], M.F. Baumgartner[a], S.A. Josey[b], A.S. Fischer[a], J.C. Kindle[c]

[a] *Woods Hole Oceanographic Institution, Woods Hole, MA 02543, USA*
[b] *Southampton Oceanography Center, Southampton, SO14 3ZH, UK*
[c] *Naval Research Laboratory, Stennis Space Center, MI 39529, USA*

Received 26 August 1997; received in revised form 25 March 1998; accepted 18 May 1998

Abstract

Accurate, year-long time series of winds, incoming shortwave and longwave radiation, air and sea temperatures, relative humidity, barometric pressure, and precipitation were collected from a surface mooring deployed off the coast of Oman along the climatological axis of the Findlater Jet from October 1994 to October 1995. Wind stress, heat flux, and freshwater flux were computed using bulk formulae. The Northeast Monsoon was characterized by steady but moderate winds, clear skies, relatively dry air, and two months, December and January, in which the ocean, on average, lost 45 $W m^{-2}$ to the atmosphere. The Southwest Monsoon had strong winds, cloudy skies, and moist air. Because of reduced latent and longwave heat loss, it was accompanied by sustained oceanic heat gain, with the strongest monthly mean warming, 147 $W m^{-2}$, in August.

Large differences are found between the observations and older climatologies. Recent climatologies agree better with the observations. The means of the Southampton Oceanography Center climatology for 1980–1995 are close to the buoy monthly means. Monthly means from that climatology show that 1994–1995 was in general a typical year, with surface meteorology and air–sea fluxes within one standard deviation of the long term means. Concurrent data from the NCEP, ECMWF, and FNMOC show that the models provide realistic surface winds. FNMOC winds show that the timing and character of the onset of the Southwest Monsoon in 1995 differed from 1994 and 1996 when variability within one month is resolved. The models fail to replicate other observed surface meteorology and to produce realistic heat

* Corresponding author. Fax: 001 508 457 2181; e-mail: rweller@whoi.edu.

0967-0645/98/$ – see front matter
PII: S0967-0645(98)00060-5

fluxes. Annual and monsoonal mean net heat fluxes from the models differed from those of the buoy by 50 to 80 $W m^{-2}$. Because of these differences, some care is warranted in selecting and using air-sea flux fields in studies of the Arabian Sea.

1. Introduction

The Arabian Sea is characterized by strong monsoonal surface forcing, which in the summer as well as in the winter is accompanied by cooling of the oceanic surface mixed layer. Many investigators have sought to understand and model the physical and biological response of the ocean there to that forcing. However, the Arabian Sea is also a data-sparse region; and the air–sea fluxes that comprise the atmospheric forcing are not well known. Year-long time series of high quality, direct observations of the near-surface meteorological variables and of the air–sea fluxes of heat, freshwater, and momentum have not been available in the central Arabian Sea. Thus, there has been some uncertainty about the role of local air–sea interaction in the observed annual evolution of upper ocean properties, including sea surface temperature and mixed layer depth. The possibility of error in present climatologies of wind stress and heat flux also has led to uncertainty about the heat balance of the Arabian Sea as a whole.

Recently, as part of a cooperative research effort in the Arabian Sea, we deployed a surface buoy off the coast of Oman at 15.5°N, 61.5°E from October 1994 to October 1995. This was done to collect accurate time series of near-surface meteorology at a site where some of the strongest winds associated with the Southwest Monsoon are found. Sensors on the buoy measured the near-surface wind, incoming shortwave and longwave radiation, barometric pressure, air temperature, sea surface temperature, relative humidity, and precipitation. These observations allow time series of the wind stress, latent heat flux, sensible heat flux, net shortwave radiation, net longwave radiation, and freshwater flux to be determined.

In this paper these year-long time series of surface meteorology and air–sea fluxes are used to describe with some certainty the atmospheric forcing at a point in the Arabian Sea characterized by strong monsoon winds. In addition, to quantify the difference between these observations and the forcing fields used in other studies, the observations and fluxes are compared with historical data and with surface fields and air–sea fluxes from numerical weather prediction models. The historical data include the Hellerman and Rosenstein (1983) (hereafter referred to as Hellerman), Hastenrath and Lamb (1979a, b) (hereafter referred to as Hastenrath), Wright (1988) and Oberhuber (1988) (collectively hereafter referred to as Oberhuber), and UWM/COADS climatologies (da Silva et al., 1994) as well as the recent Southampton Oceanography Center analysis of the COADS reports from 1980 to 1995 (Josey et al., 1996, 1998) (hereafter referred to as SOC 1980–1995). The numerical weather prediction model data come from the operational analyses carried out at ECMWF (European Centre for Medium Range Weather Forecasting) and FNMOC (Fleet Numerical

Meteorology and Oceanography Center) and the reanalysis conducted at NCEP (National Centers for Environmental Prediction). The buoy data were not included in either the observations used to create the climatologies or the surface meteorological data assimilated by the models.

2. Arabian Sea surface buoy

The location chosen for the surface mooring, 15.5°N, 61.5°E, was close to the climatological maximum in the wind speed during the height of the Southwest Monsoon. Two separate mooring deployments, the first beginning October 15, 1994, and ending April 20, 1995, and the second starting April 22, 1995, and ending October 10, 1995, were used so that a second set of freshly calibrated sensors was deployed prior to the onset of the Southwest Monsoon. A brief discussion of the meteorological instrumentation is provided here; more information about the design of the mooring, the deployment cruises, and the moored instrumentation is provided in Trask and Weller (1995), Trask et al. (1995a, b), Ostrom et al. (1996), and Baumgartner et al. (1997).

The 3-m diameter surface buoy (Fig. 1) carried two separate, complete meteorological instrument packages and a third package that measured just humidity and air temperature. Table 1 summarizes the sensors associated with the different instruments, their heights and sampling characteristics. One instrument was the Vector-Averaging Wind Recorder or VAWR (Weller et al., 1990), recording every 7.5 min; and the other was the Improved Meteorological Recorder or IMET (Hosom et al., 1995), recording every minute. The additional Rotronic MP-100 humidity and air temperature sensor was sampled by a third, independent or "stand-alone" data logger.

The shortwave and longwave radiometers were the highest sensors, located away from shadows. The Eppley longwave radiometers were modified so that thermopile, body, and dome temperatures could be recorded and, in later processing, used for computing incoming longwave radiation. The buoy was fitted with a large vane so that it would have a preferred orientation with respect to the wind. The sensors needing ventilation (air temperature and relative humidity) and undisturbed airflow (wind speed and wind direction) were placed on the windward side of the buoy. In low winds the buoy vane does not always develop sufficient torque to bring the front face of the sensor array into the wind, and the passive Gill multiplate radiation shields (Gill, 1983) do not entirely prevent radiative heating from influencing the air temperature measurements (Payne, 1987). To overcome these problems, which were likely to occur in the intermonsoon periods, an additional air temperature sensor was installed with an electrically driven fan to provide aspiration. As space on the buoys for batteries was limited, there was only power to run the aspirator for approximately the first two months of each deployment, when low wind and significant radiative heating errors were anticipated. Anderson and Baumgartner (1998) developed the empirical algorithm used here to correct the non-aspirated air temperature, reducing the radiative heating error to at most 0.3°C.

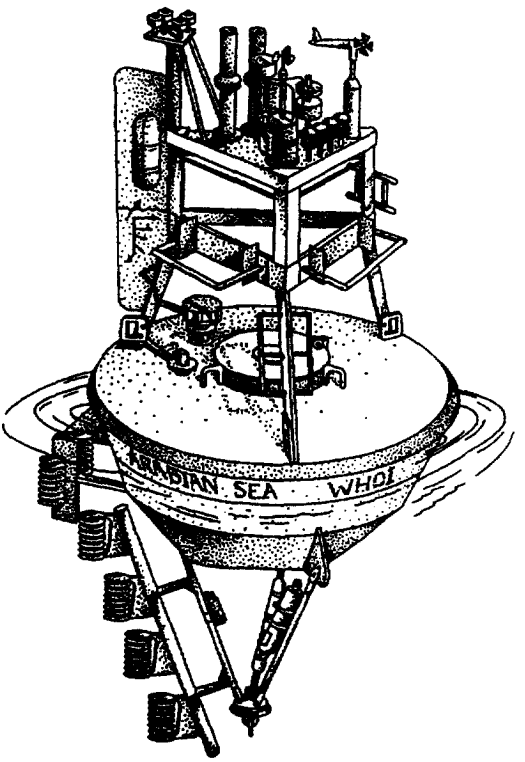

Fig. 1. Line drawing of the buoy deployed in the Arabian Sea, showing meteorological sensors on the superstructure and shallow ocean temperature sensors to the side and below the hull.

The performance of the meteorological instruments and individual sensors was examined by comparison with separate transfer standards in Woods Hole prior to shipment, after re-assembly in the port of Muscat in Oman, at sea just following deployment, and just prior to recovery. In Woods Hole, before and after the deployments, all sensors were recalibrated in the laboratory except for the radiometers, which were returned to Eppley for recalibration. In addition, the shortwave radiometers were sent to the Electric Power Research Institute in Colorado for comparison with their standard radiometers. No significant shifts in any calibrations were observed, and the data were processed using the pre-deployment calibrations. Checks of the quality of the processed data were made by comparing the VAWR, IMET, and stand-alone data sets. Shipboard meteorological data were collected immediately following buoy deployments and just prior to buoy recoveries using both a set of recently calibrated meteorological sensors mounted on the jackstaff of the R/V *Thomas Thompson* and the ship's standard set of IMET sensors. These observations provided an independent data set that was compared to the data from the buoy.

Table 1
Summary of meteorological sensors deployed on the WHOI buoy. Heights are reported in meters above the mean water line. The rate at which data was recorded was every 7.5 min for the VAWR and every 1 min for the IMET. Most measurements are an average over the recording period; but some, as noted in the table, are an average over a shorter interval within the recording period

Parameter	Sensor	Height (m)	Sampling characteristics
VAWR			
Air temperature	thermistor	2.68	1.875 min average
Relative humidity	Väisäla Humicap	2.69	3.515 s sample
Barometric pressure	Paroscientific Digiquartz	2.76	2.636 s sample
Wind speed/direction	cup/vane	3.63/3.07	7.5 min vector average
Shortwave radiation	Eppley 8-48	3.42	7.5 min average
Longwave radiation	Eppley PIR	3.42	7.5 min average
Sea temperature	thermistor	−0.92	1.875 min average
IMET			
Air temperature	Platinum resistance	2.74	1 min average
Relative humidity	Rotronic MP-100	2.74	1 min average
Barometric pressure	AIR DB-1A	2.77	1 min average
Wind speed/direction	R.M. Young 5103	3.16	1 min vector average
Shortwave radiation	Eppley PSP	3.42	1 min average
Longwave radiation	Eppley PIR	3.42	1 min average
Precipitation	R.M. Young siphon	3.14	1 min sample
Aspirated air temperature	Platinum resistance	2.20	1 min average
Stand-alone			
Air temperature	Rotronic MP-100	2.98	3.5 s sample
Relative humidity	Rotronic MP-100	2.98	3.5 s sample

Only one sensor failed, and this was the barometric pressure sensor on the VAWR used in the second deployment. From the IMET and VAWR data, the best time series were selected and used to make one set of time series of surface meteorology with 7.5 min sampling. The choice of which data were best was based both on sensor performance and on minimizing error in quantities to be computed from the basic observations. For example, the IMET longwave radiation sensors showed greater error due to heating by the sunlight, so the VAWR longwave data were used. In the case of relative humidity, the IMET relative humidity time series was selected because that sensor had a collocated temperature sensor and allowed a more accurate computation of specific humidity. More detail about the preparation of the one-year meteorological time series is provided in Baumgartner et al. (1997).

The calibrations and comparisons, together with previous experience in the TOGA Coupled Ocean Atmosphere Response Experiment (COARE) (Weller and Anderson, 1996), led to the summary of measurement accuracy for monthly means provided by Table 2. The air–sea fluxes were computed following procedures summarized in Weller and Anderson (1996), with the sign convention that a negative value for heat

flux indicates oceanic heat loss. Wind stress, latent heat flux, and sensible heat flux were calculated using version 2.5 of the bulk formulae developed during COARE, described by Fairall et al. (1996a). For the flux computations the shallowest (0.17 m) temperature observations were extrapolated to the surface to obtain a skin temperature (Fairall et al., 1996b). Net shortwave radiation was computed from incoming shortwave radiation using a variable albedo based on the solar elevation angle and an atmospheric transmittance of 0.720 (Payne, 1972). Net longwave radiation was computed by subtracting an estimate of the outgoing longwave, $LW\uparrow = \varepsilon\sigma T^4 + (1 - \varepsilon)LW\downarrow$, from the measured incoming longwave, $LW\downarrow$, where the emissivity, ε, was chosen to be 0.97, and σ is the Stefan–Boltzmann constant ($5.67 \times 10^{-8}\,W\,m^{-2}\,K^{-4}$). Freshwater flux was calculated by combining the observed precipitation rate with evaporation calculated from the latent heat flux.

3. Meteorology and air-sea fluxes at the buoy

Both sea and air temperature showed two periods of cooling, December 1994 through February 1995 and from June 1995 through July 1995. This can be seen in both the time series of surface meteorology (Fig. 2) and in monthly means of those time series (Table 3). The high wind stress of the Southwest Monsoon is evident in the times series of the air–sea fluxes (Fig. 3) and in the monthly means of the observed

Table 2
Abbreviations, units and estimated accuracies of the meteorological observables and air–sea fluxes

Parameter	Units	Abbreviation	Typical accuracy
Meteorological observables			
Wind speed	$m\,s^{-1}$	U	5%
Wind direction	Degrees	WD	10°
Barometric pressure	mbar	BP	0.5 mbar
Air temperature	°C	AT	0.1°C
Sea surface temperature	°C	SST	0.1°C
Incoming shortwave radiation	$W\,m^{-2}$	$SW\downarrow$	3%
Incoming longwave radiation	$W\,m^{-2}$	$LW\downarrow$	$10\,W\,m^{-2}$
Relative Humidity	%	RH	4%
Specific Humidity	$g\,kg^{-1}$	SH	$0.2\,g\,kg^{-1}$
Precipitation	$mm\,h^{-1}$	P	$0.01\,mm\,h^{-1}$
Air–sea fluxes			
Sensible heat flux	$W\,m^{-2}$	Q_{sen}	$2\,W\,m^{-2}$
Latent heat flux	$W\,m^{-2}$	Q_{lat}	$5\,W\,m^{-2}$
Net shortwave radiation	$W\,m^{-2}$	SW_{net}	$10\,W\,m^{-2}$
Net longwave radiation	$W\,m^{-2}$	LW_{net}	$5\,W\,m^{-2}$
Net heat flux	$W\,m^{-2}$	Q_{net}	$15\,W\,m^{-2}$
Wind stress	$N\,m^{-2}$	$\lvert\tau\rvert$	$0.01\,N\,m^{-2}$
Freshwater Flux	$mm\,h^{-1}$	E-P	$0.01\,mm\,h^{-1}$

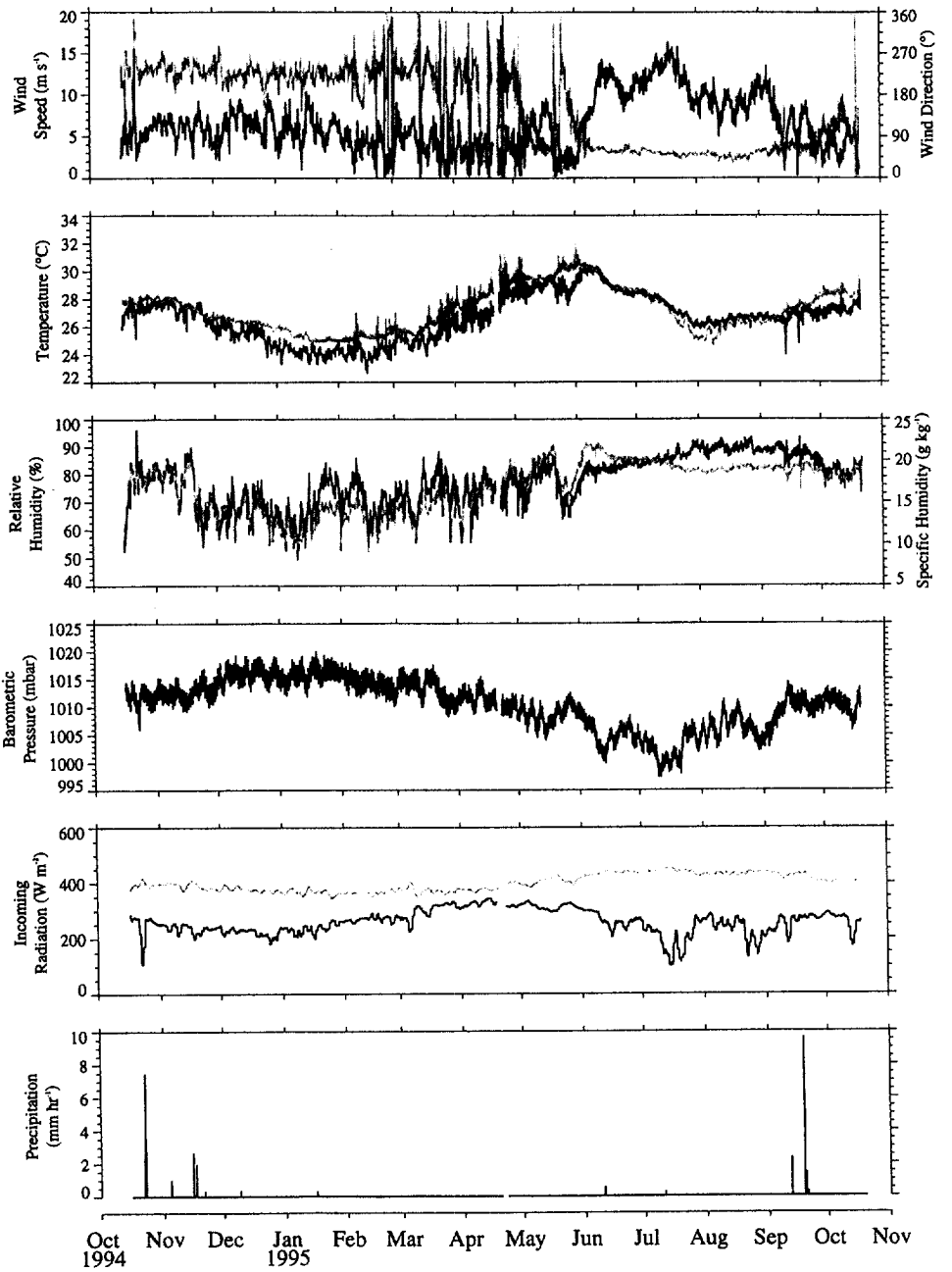

Fig. 2. Time series of meteorological observables from the Arabian Sea buoy. From top to bottom, overplot of wind speed (black) and wind direction (gray, toward, so that 0° is flow to the north and 90° is flow to the east), overplot of air (black) and sea surface (gray) temperatures, overplot of relative (solid) and specific (gray) humidities, barometric pressure, overplot of incoming longwave radiation (gray) and incoming shortwave radiation (solid), and precipitation rate. All are one-hour averages, except incoming shortwave and longwave, which have been low-pass filtered with a 48-h running mean.

Table 3
Monthly averaged values and the annual (October 1994–October 1995) means of the meteorological observables from the WHOI mooring at 15.5°N, 61.5°E

Month	U	WD	AT	SST	RH	SH	BP	SW↓	LW↓	P
Oct. 94[a]	5.29	234	27.24	27.91	77.0	17.55	1011.6	250.5	393.9	0.0557
Nov. 94	6.26	237	27.23	27.52	75.6	17.01	1012.7	237.2	390.8	0.0099
Dec. 94	6.64	227	25.53	26.34	67.1	13.59	1015.8	221.9	377.0	0.0005
Jan. 95	6.03	223	24.21	25.30	67.6	12.61	1015.8	237.0	367.1	0.0004
Feb. 95	3.95	227	24.19	25.35	69.9	13.00	1014.1	270.5	367.2	0.0000
Mar. 95	4.26	226	25.30	26.25	73.2	14.47	1013.2	300.6	372.9	0.0000
Apr. 95	3.17	226	27.19	28.47	74.0	16.46	1011.2	318.9	383.2	0.0000
May. 95	4.46	103	28.86	29.84	75.9	18.73	1008.7	313.5	406.7	0.0000
Jun. 95	9.91	66	29.25	29.45	82.3	20.69	1005.2	264.8	436.4	0.0008
Jul. 95	12.37	54	27.42	27.00	86.3	19.37	1002.5	198.1	440.6	0.0004
Aug. 95	9.33	50	26.46	25.93	89.6	18.94	1006.2	230.2	432.0	0.0000
Sep. 95	6.82	66	26.77	27.21	87.5	18.90	1009.4	255.6	421.6	0.0230
Oct. 95[b]	3.88	108	27.26	28.41	80.6	18.16	1010.4	259.0	406.7	0.0000
Annual	6.50	157	26.65	27.24	77.4	16.83	1010.4	258.0	400.0	0.0053

[a] Includes data from October 16, 1994, to October 31, 1994, only.
[b] Includes data from October 1, 1995, to October 19, 1995, only.

fluxes (Table 4). The Northeast Monsoon (averages from November 1, 1994 to February 15, 1995 are given in Table 5) was characterized by steady but moderate winds, clear skies, relatively dry air, and two months, December and January, in which the ocean, on average, lost 45 $W m^{-2}$ to the atmosphere. The Southwest Monsoon (averages from June 1 to September 15, 1995 are given in Table 5) had strong winds, cloudy skies, and moist air. Because of reduced latent and longwave heat loss, it was accompanied by sustained oceanic heat gain, with the strongest monthly mean warming, 147 $W m^{-2}$, in August.

The variability associated with the monsoons was a major signal in the observed surface meteorology, though an annual cycle was seen in the incoming shortwave radiation. Wind direction was towards the southwest, at an average heading of 228°, during the Northeast Monsoon; and wind speed averaged 6.05 $m s^{-1}$. Wind speeds were lower and wind direction more variable during the March through May intermonsoon period. At the onset of the Southwest Monsoon the wind speed rose initially in early May, then became light, before rising again in early June. The timing of both wind speed increases matches that found by Fieux and Stommel (1977) during years they characterize as having multiple onsets. During the Southwest Monsoon wind speed averaged 10.16 $m s^{-1}$ and wind direction, 57°. Peak wind speeds during the Northeast Monsoon were 10.9 $m s^{-1}$ on January 16, 1995 and during the Southwest Monsoon, 18.3 $m s^{-1}$ on July 21, 1995. The wind direction was very steady during the Southwest Monsoon; the ratio of vector to scalar wind speeds was 0.987 and the standard deviation of the scalar wind speed was 2.72 $m s^{-1}$ or 26.8% of the

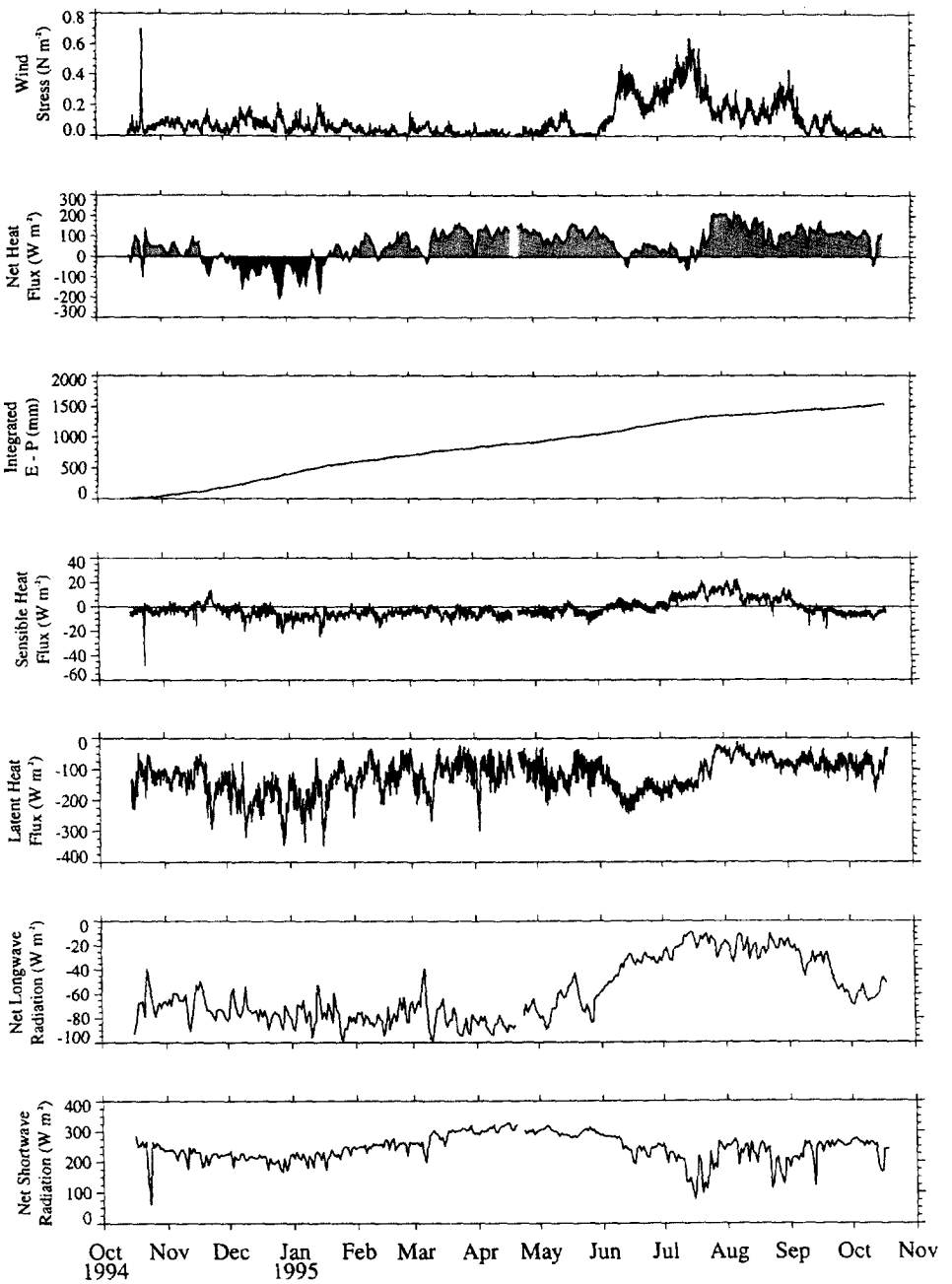

Fig. 3. Time series of the air–sea fluxes computed using the data in Fig. 2 and bulk formulae. From top to bottom, the magnitude of the wind stress, net heat flux, time-integrated net freshwater flux (E-P), sensible heat flux, latent heat flux, net longwave radiation, and net shortwave radiation. All are one-hour averages except net heat flux and net shortwave and longwave radiation, which have been low-pass filtered with a 48-h running mean. Positive heat fluxes indicate ocean heating.

Table 4
Monthly averaged values and the annual (October 1994–October 1995) means of the estimated air–sea fluxes at the WHOI mooring at 15.5°N, 61.5°E

Month	$\|\tau\|$	Q_{sen}	Q_{lat}	SW_{net}	LW_{net}	Q_{net}	E-P
Oct. 94[a]	0.0597	−3.9	−120.5	235.9	−68.4	43.0	0.1212
Nov. 94	0.0724	0.0	−136.2	222.1	−69.1	16.8	0.1900
Dec. 94	0.0860	−5.7	−196.9	206.7	−75.1	−71.0	0.2886
Jan. 95	0.0662	−7.6	−171.0	221.3	−78.6	−36.0	0.2506
Feb. 95	0.0291	−5.4	−110.7	254.0	−78.8	59.1	0.1625
Mar. 95	0.0354	−4.2	−112.1	283.9	−78.7	88.8	0.1646
Apr. 95	0.0191	−5.0	−97.8	301.9	−81.8	117.3	0.1435
May. 95	0.0436	−3.7	−114.9	297.0	−67.4	111.0	0.1686
Jun. 95	0.2123	0.1	−165.5	251.0	−37.0	48.7	0.2421
Jul. 95	0.3248	9.0	−122.4	188.0	−18.6	56.0	0.1792
Aug. 95	0.1706	8.9	−59.8	218.8	−20.8	147.0	0.0877
Sep. 95	0.1008	−1.8	−80.7	242.1	−38.0	121.6	0.0954
Oct. 95[b]	0.0266	−5.6	−87.2	244.3	−59.0	92.4	0.1280
Annual	0.1007	−1.7	−122.6	243.3	−58.7	60.3	0.1747

[a] Includes data from October 16, 1994, to October 31, 1994, only.
[b] Includes data from October 1, 1995, to October 19, 1995, only.

Table 5
Average values of the meteorological observables and air-sea fluxes for the Northeast Monsoon (November 1, 1994, through February 15, 1995, inclusive), and the Southwest Monsoon (June 1 through September 15, 1995, inclusive)

Variable	NE Monsoon	SW Monsoon
Observables		
U	6.05	10.16
WD	228	57
AT	25.43	27.54
SST	26.21	27.34
RH	70.3	86.4
SH	14.23	19.54
BP	1014.8	1005.2
$SW\downarrow$	237.3	232.0
$LW\downarrow$	376.0	435.1
P	0.0030	0.0012
Air–sea fluxes		
$\|\tau\|$	0.0693	0.2221
Q_{sen}	−4.7	5.3
Q_{lat}	−161.3	−110.0
SW_{net}	221.8	220.2
LW_{net}	−75.4	−26.0
Q_{net}	−19.7	89.5
E-P	0.2337	0.1603

mean. During the Northeast Monsoon the ratio of vector to scalar wind speeds was 0.937, and the standard deviation was 1.61 $m s^{-1}$ or 26.6% of the mean.

Low-passed, incoming shortwave radiation showed an annual cycle with a maximum during the intermonsoon in April. The observed annual variability in the low-passed incoming shortwave was only roughly approximated by low-passed, clear sky, incoming shortwave radiation calculated from the formulae in the Smithsonian Meteorological Tables (List, 1984) using an atmospheric transmission coefficient of 0.72 (Fig. 4). From October 1994 to mid-April 1995 the calculated and observed daily integrated incoming shortwave radiation agreed to within approximately 10%. However, the difference between the observed and calculated shortwave was large during the Southwest Monsoon due to increased cloud cover. Incoming longwave radiation varied over the year, averaging to 390 $W m^{-2}$ from the deployment in October through to the intermonsoon in May and then rising to an average of 435 $W m^{-2}$ during the Southwest Monsoon.

Humidity was lowest and showed considerable variability (standard deviation of 8.0%) during the Northeast Monsoon, when relative humidity dropped at one point to 47.3% (specific humidity to 8.6 g kg^{-1}) and averaged 70.3%. In contrast, the average relative humidity during the Southwest Monsoon was higher at 86.4%, rose steadily from June through late August, and had much less variability (standard deviation of 3.5%). Rain was observed only during the fall in association with synoptic weather events. There were a total of six such occasions, in October and November 1994 and in September 1995. The most dramatic such event, a low pressure system in October 1994, had 21.4 mm of accumulated rain, winds in excess of 17 $m s^{-1}$, and dense cloud cover associated with it. Total accumulated rainfall over the year was 46.6 mm.

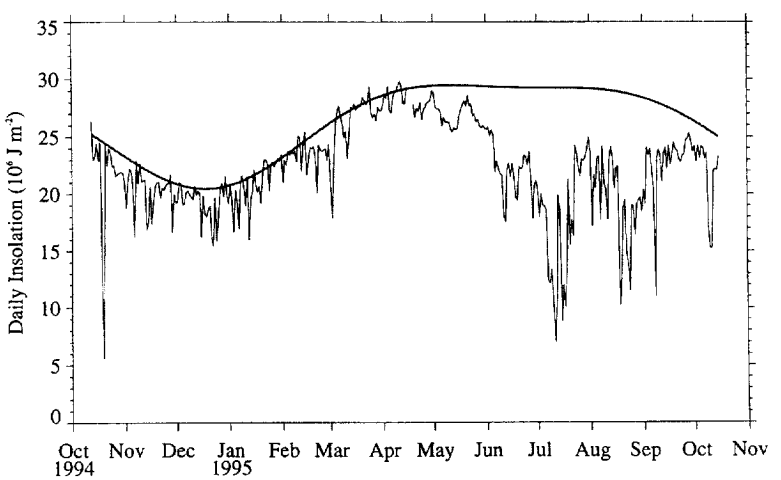

Fig. 4. Comparison of the daily-integrated, clear-sky incoming shortwave radiation computed for 15.5°N, 61.5°E (thicker, gray line) using an atmospheric transmission coefficient of 0.72 with the observed daily-integrated incoming shortwave radiation (thin, black line).

Variability in the air–sea fluxes also showed monsoonal and annual signals. The wind stress peaked in July during the Southwest Monsoon. Air temperature was typically cooler (0.59°C on average) than the sea surface temperature with the exception of the period from mid-July through to the beginning of September (the height of the Southwest Monsoon), when the air temperature was up to 1.71°C and, on average, 0.36°C warmer than the sea surface temperature. Thus, the sensible heat flux, while relatively small in both monsoons, was of opposite sign. Latent heat flux was large throughout the Northeast Monsoon. During the Southwest Monsoon it initially increased with the wind speed, but dropped to close to zero in late July. In contrast to net longwave radiation, which decreased by $50\,W\,m^{-2}$ during the Southwest Monsoon, the average net shortwave radiation had essentially the same value during the two monsoons. With only brief rain events each fall, the freshwater flux (E-P) was dominated by evaporation and had an annual mean of $0.175\,mm\,h^{-1}$.

Over the whole year, the low-passed net heat flux was negative (oceanic heat loss) during the isolated storm in October 1994, during late November, from early December through mid-January, again later in mid-January, for brief periods in February and March, for two periods of several days each during June and July, and again once in October 1995. The mean net heat flux for the Northeast Monsoon (Table 5) was an oceanic loss, $-19.7\,W\,m^{-2}$, while that during the Southwest Monsoon was an oceanic gain, $89.5\,W\,m^{-2}$. The heat gain of the Southwest Monsoon resulted largely from reductions in both the latent heat loss and in the net longwave radiative loss relative to those seen during the Northeast Monsoon. The largest oceanic heat gains of the whole year, as indicated by the low-passed net heat fluxes, were in fact observed in the later half of the Southwest Monsoon.

Air–sea temperature and humidity differences and cloud cover, as well as wind speed, contributed to the variability observed in the air–sea fluxes. Throughout the Northeast Monsoon, the sea surface temperature was warmer than the air temperature. With the relatively dry air off Asia cooler than the sea surface temperature, a strong near-surface gradient in specific humidity (the average difference between the observed and saturated specific humidity was $-6.6\,g\,kg^{-1}$) was maintained and the latent heat loss was large even though wind speeds were moderate. In contrast, during the Southwest Monsoon the air arriving at the mooring was moister and close to, and at times warmer than, the sea surface temperature. That sea-surface temperature was also warmer than during the Northeast Monsoon. As a result, the near-surface specific humidity gradient during the Southwest Monsoon was small (the average difference between the observed and the saturated specific humidity was $-2.9\,g\,kg^{-1}$), particularly so when the air temperature was warmer than the sea surface temperature, and thus the latent heat flux was reduced even though the wind speeds were much greater than during the Northeast Monsoon. Cloudy, moist conditions also reduced the net longwave heat loss by the ocean. In spite of strong winds during the Southwest Monsoon, only on two occasions did increased cloud cover and reduction in net shortwave radiation shift the daily-averaged net heat flux to oceanic loss, and then only for several days in duration.

4. Comparisons with ship-based and model fields

In this section the buoy observations are compared against data from various other sources. First, the differences between various climatologies (whose mean fields are built up primarily from many years of ship reports) and the buoy observations are examined, focusing on the monsoon periods (Section 4.1). When looking at a particular year instead of average conditions, the surface meteorology and air–sea fluxes from numerical weather prediction models provide convenient, gridded fields with good temporal resolution. To examine how well models replicate the observations, the buoy time series are also compared (Section 4.2) with concurrent time series from the ECMWF, NCEP, and FNMOC numerical weather prediction models.

4.1. Comparison with climatological data

While the several climatologies chosen as representative have seen frequent use, the SOC 1980–1995 flux data set may be less familiar. The SOC 1980–1995 fields result from the analysis of an enhanced COADS data set for the period 1980–1995 containing additional metadata describing observing procedures on the reporting ships that has allowed various observational biases to be removed. The SOC 1980–1995 data used here are an extended version of those used to produce the SOC climatology (Josey et al., 1998) based on the period 1980–1993. The two-year extension allows us to address the question of whether the buoy deployment period was typical. The SOC 1980–1995 data used here were obtained by extracting and averaging the 25 $1^\circ \times 1^\circ$, analyzed, mean values contained within a 5° square centered on the buoy. Additional comparisons, not presented here, were done for the single $1^\circ \times 1^\circ$ square centered on the buoy; and similar results were obtained although the time series tended to be more noisy due to the low sampling at this resolution. The Hellerman wind stresses and Oberhuber surface meteorology and fluxes come from a $2^\circ \times 2^\circ$ box centered at 15°N, 61°E, 41.7 km away from the mooring site. The Hastenrath and the UWM/COADS data come from a $1^\circ \times 1^\circ$ box centered on the mooring.

These various climatologies differ in the annual mean (Table 6) and during both monsoons (Table 7). To simplify calculations using monthly values, the two monsoon periods were defined for this comparison to be November, December, and January for the Northeast Monsoon and June, July, and August for the Southwest Monsoon. Also included in Table 7 are the buoy means for the same periods in 1994–1995 together with the means of the SOC data for 1994–1995 (hereafter referred to as SOC 1994–1995). Interpretation of Tables 6 and 7 is made difficult because different methods and sampling periods have been used to produce each of the climatologies. In addition, the buoy data only sampled a one year period. However, interesting conclusions still can be drawn, particularly about biases in some of the climatologies. This is not a detailed comparison of the different climatologies in terms of methods used for their generation; our goal is to identify major differences in the picture of the net heat exchange in this region that would result from using these different climatologies.

Table 6
Annual means of the meteorological observables and air–sea fluxes from the buoy and the climatologies. Data from SOC for the period matching the buoy deployment is labeled SOC 1994–1995, while the climatological means are SOC 1980–1995. UWM/COADS constrained heat flux is in parentheses

	1994–1995		Climatology			
	Buoy	SOC 1994–1995	SOC 1980–1995	UWM COADS	Hastenrath	Oberhuber
U_{10m}	7.1	7.6	7.3	6.2	5.8	6.7
WD	157	164	153	150		173
AT_{10m}	26.6	26.6	26.4	26.8	26.4	26.8
SST	27.2	26.9	27.0	27.0	26.6	27.0
RH_{10m}	75.8	79.8	78.8	79.0	78.3	78.9
SH_{10m}	16.4	17.2	16.8	17.2	16.7	17.2
BP	1010.4	1010.8	1010.9	1010.6	1010.5	1010.5
P	0.0053	0.0053	0.0234	0.0279		0.0317
$\|\tau\|$	0.1007	0.1166	0.1080	0.0869		
Q_{sen}	−1.7	−1.2	−2.7	−2.8	−0.2	0.0
Q_{lat}	−122.6	−112.7	−117.3	−112.0	−107.9	−113.6
SW_{net}	243.3	241.1	240.0	243.5	199.2	202.3
LW_{net}	−58.7	−66.0	−68.3	−51.5	−62.1	−51.1
Q_{net}	60.3	61.3	51.6	77.3 (39.0)	29.0	37.9
E-P	0.1747	0.1600	0.1488	0.1380		0.1254

Note: The Hellerman and Rosenstein (1983) value for $|\tau|$ is 0.1308 N m^{-2}.

Table 7a
Observed and climatological means during the Northeast Monsoon (November, December, and January). UWM/COADS constrained heat flux is in parentheses

	1994–1995		Climatology			
	Buoy	SOC 1994–1995	SOC 1980–1995	UWM COADS	Hastenrath	Oberhuber
U_{10m}	6.9	6.8	6.3	5.5	5.2	5.6
WD	229	225	222	219		222
AT_{10m}	25.5	25.9	25.4	25.8	25.3	25.9
SST	26.4	26.1	26.3	26.3	26.0	26.4
RH_{10m}	68.3	72.5	74.1	73.3	70.0	73.5
SH_{10m}	13.8	14.9	14.8	15.0	13.8	15.2
BP	1014.8	1015.6	1014.8	1014.7	1014.6	1014.4
P	0.0035	0.0083	0.0167	0.0207		0.0308
$\|\tau\|$	0.0749	0.0675	0.0598	0.0502		
Q_{sen}	−4.5	−1.2	−5.3	−6.4	−5.3	−3.6
Q_{lat}	−168.4	−150.2	−145.8	−141.4	−123.3	−128.3
SW_{net}	216.6	188.3	195.7	192.8	168.3	165.9
LW_{net}	−74.3	−76.2	−81.9	−62.2	−71.7	−59.8
Q_{net}	−30.6	−39.4	−37.3	−17.3 (−54.5)	−32.0	−25.7
E-P	0.2436	0.2122	0.1973	0.1886		0.1453

Note: The Hellerman and Rosenstein (1983) value for $|\tau|$ in the NE monsoon is 0.0668 N m^{-2}.

Table 7b
Observed and climatological means during the Southwest Monsoon (June, July, and August). UWM/COADS constrained heat flux is in parentheses

	1994–1995		Climatology			
	Buoy	SOC 1994–1995	SOC 1980–1995	UWM COADS	Hastenrath	Oberhuber
U_{10m}	11.6	12.7	12.4	12.5	12.0	12.5
WD	57	51	52	53		48
AT_{10m}	27.7	27.4	27.2	27.4	26.9	27.2
SST	27.4	27.2	27.1	27.1	26.8	26.9
RH_{10m}	84.3	86.8	83.3	85.3	87.3	84.5
SH_{10m}	19.4	19.6	18.6	19.3	19.2	18.9
BP	1004.6	1005.0	1005.5	1004.7	1004.7	1004.9
P	0.0004	0.0093	0.0462	0.0440		0.0471
$\|\tau\|$	0.2362	0.3007	0.2843	0.2370		
Q_{sen}	6.0	4.0	2.6	2.6	8.0	6.9
Q_{lat}	−115.3	−115.6	−128.0	−122.8	−146.7	−166.2
SW_{net}	218.9	240.3	229.0	231.8	171.7	192.8
LW_{net}	−25.4	−41.4	−39.7	−33.9	−45.0	−36.8
Q_{net}	84.3	87.3	64.0	77.7 (36.5)	−12.0	−3.3
E-P	0.1689	0.1603	0.1417	0.1381		0.1820

Note: The Hellerman and Rosenstein (1983) value for $|\tau|$ in the SW Monsoon is 0.3779 $N m^{-2}$.

The climatological means of the meteorological variables are mostly in broad agreement and the differences between their monthly means and those of the buoy data show similar patterns of variability over the annual cycle (Fig. 5). The SOC 1980–1995 mean wind speed in the Northeast Monsoon (6.3 $m s^{-1}$) is typically about 10% greater than that found in the other climatologies, but not during the Southwest Monsoon. The differences among the climatological monthly means in the sea surface and air temperatures are up to 0.5°C, and in the air–sea temperature differences are up to 0.4°C. Differences in monthly mean specific humidity reach 2 $g kg^{-1}$ but are typically between 0.5 and 1 $g kg^{-1}$.

Larger differences are found among the climatological fluxes due to the various empirical formulae employed (Fig. 6). Better general agreement is seen between the buoy and SOC 1980–1995 fluxes, particularly the net heat flux, than between the buoy and other climatologies. The large magnitude of the wind stress obtained by Hellerman for the Southwest Monsoon, 0.380 $N m^{-2}$, is probably due to their use of a simple drag coefficient parameterization, which has values at high wind speeds that are significantly greater than those obtained with detailed experimental analyses (Smith, 1980). Differences in the monthly means of the sensible heat flux are small, under 10 $W m^{-2}$. Sensible heat flux is a relatively small term in the overall heat budget in all of the climatologies considered.

The dominant terms in the heat exchange, latent heat flux and shortwave radiation, show larger differences. The various estimates of the latent heat flux range from − 120

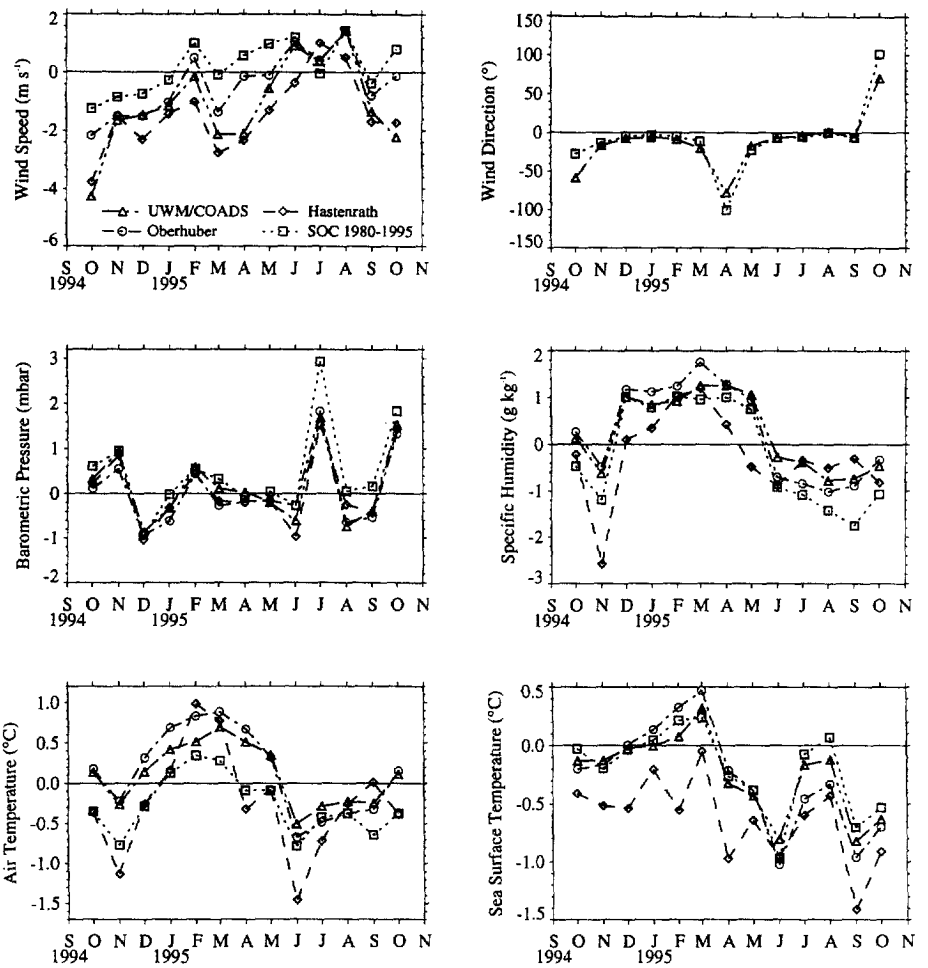

Fig. 5. Overplots of the differences between monthly means of the buoy observations and the UWM/COADS, Hastenrath, Oberhuber, and SOC 1980–1995 climatologies. The difference is computed as (climatology–buoy value). Different symbols and line types are used as indicated in the overplot of the wind speeds.

to $-150\ \mathrm{W\,m^{-2}}$ during each monsoon, though Oberhuber shows more loss in the Southwest Monsoon. The SOC 1980–1995 and UWM/COADS latent heat fluxes (computed using stability dependent parameterizations of the transfer coefficients for the heat loss rather than the constant value used in Hastenrath) are closer to the buoy monthly means. The monthly cloud cover values from UWM/COADS, Hastenrath, and Oberhuber show large increases in cloud cover from May to August, consistent with the reduction in incoming shortwave radiation seen at the buoy during the Southwest Monsoon. Climatological estimates of the net shortwave radiation range

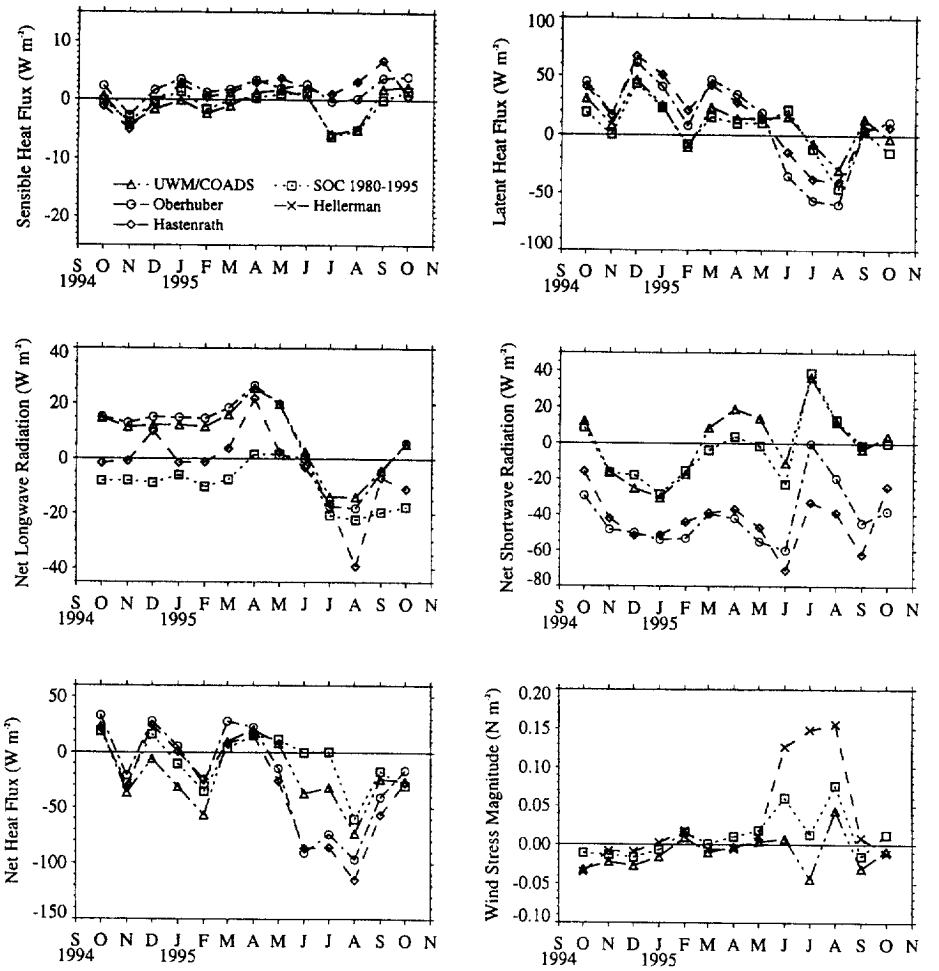

Fig. 6. Overplots of the differences between monthly mean fluxes at the buoy and the UWM/COADS, Oberhuber, Hastenrath, SOC 1980–1995, and Hellerman climatologies. The difference is computed as (climatology–buoy value). Different symbols and line types are used as indicated in the overplot of the sensible heat fluxes.

from 166 to 196 W m^{-2} for the Northeast Monsoon and from 172 to 232 W m^{-2} for the Southwest. There is a distinct difference between the Oberhuber and Hastenrath climatologies and the SOC 1980–1995 and UWM/COADS climatologies; the earlier climatologies have monthly means of net shortwave radiation that are lower by 20–50 W m^{-2}. The buoy monthly means agree better with the higher values found in the SOC 1980–1995 and UWM/COADS analyses.

Differences in the net longwave radiation are smaller but still significant, as their value can change the sign of the net heat flux. Estimates of the longwave radiation in

the Northeast Monsoon range from -60 to $-82\,W\,m^{-2}$ and from -34 to $-45\,W\,m^{-2}$ in the Southwest Monsoon. The SOC 1980–1995 estimates of net longwave radiation used in the current analysis were obtained with the Bignami et al. (1995) formula, which is based on measurements made in the Mediterranean Sea with an appreciable proportion of clear sky conditions. We note that the formula of Clark et al. (1974) is thought to be more applicable under mid-latitude, high cloud cover conditions (Josey et al., 1997) and was used to produce a 1980–1993 global SOC climatology (Josey et al., 1998). The close agreement between the buoy measured net longwave radiation ($-74.3\,W\,m^{-2}$) for the Northeast Monsoon and the SOC 1994–1995 estimate ($-76.2\,W\,m^{-2}$) suggests that the Bignami et al. (1995) formula is indeed the more appropriate choice under conditions of low cloud cover. The greater cloud cover conditions experienced at the buoy during the Southwest Monsoon led all of the climatological estimates for the net longwave radiation to be greater losses than the buoy value by -10 to $-20\,W\,m^{-2}$.

Of particular interest is the net atmosphere–ocean heat flux during the two monsoons. During the Northeast Monsoon the climatological estimates all indicate a heat loss by the ocean of between -17 and $-37\,W\,m^{-2}$; the values from the buoy and SOC 1994–1995 are losses of -30.6 and $-39.4\,W\,m^{-2}$, respectively. The situation is somewhat different during the Southwest Monsoon. The buoy shows a significant heat gain by the ocean of $84.3\,W\,m^{-2}$, in close agreement with the SOC 1994–1995 value, $87.3\,W\,m^{-2}$. The climatological estimates from UWM/COADS ($77.7\,W\,m^{-2}$) and SOC 1980-1995 ($64.0\,W\,m^{-2}$) are smaller but still indicate a significant heat gain during the Southwest Monsoon. In contrast, both the Hastenrath and the Oberhuber analyses indicate heat loss with values of -12.0 and $-3.3\,W\,m^{-2}$, respectively. The reason for this difference lies principally in the weaker shortwave gain and stronger latent heat loss in the older climatological analyses. Finally, note that the value in parentheses in the UWM/COADS column in the tables is the "constrained" net heat flux, which has been determined by adjusting the various components of the heat flux within the framework of a simple linear inverse analysis with the constraint that the global net heat flux must average to zero. With this approach values of -54.5 and $36.5\,W\,m^{-2}$ are obtained for the climatological Northeast and Southwest Monsoons, respectively, leading to greater disagreement with the buoy estimates than was the case with the original unconstrained estimates.

The freshwater flux is dominated by evaporation. In the SOC 1980–1995, UWM/COADS, and Oberhuber climatologies the annual average precipitation rates are between 16 and 25% of the freshwater flux. The annual precipitation rate observed at the buoy was only 3% of the freshwater flux. The climatological rain rates are 4 to 6 times larger than the buoy precipitation rate; and, in spite of the dominance of evaporation, these rain rate differences contribute significantly to the difference between the buoy and the climatological freshwater flux. The remainder of the difference stems from biases in the climatological latent heat fluxes, which are especially apparent in the comparison of the fluxes during the Northeast and Southwest Monsoons (Tables 7a and 7b). Both SOC 1980–1995 and UWM/COADS indicated a larger freshwater flux during the Northeast Monsoon than during the Southwest Monsoon while Oberhuber indicated the opposite. The buoy observations

and SOC 1994–1995 showed much less precipitation than the climatologies during both monsoons, but support the SOC 1980–1995 and UWM/COADS climatologies with larger freshwater fluxes during the Northeast Monsoon than during the Southwest Monsoon.

4.2. Comparison with concurrent fields

The buoy meteorological data and air–sea fluxes were compared to the concurrent surface meteorology and air–sea fluxes from SOC 1994–1995 as well as from numerical weather prediction models from ECMWF, NCEP, and FNMOC. This comparison was done, in part, to learn how best to assemble forcing fields for the Arabian Sea in 1994–1995 that would be, at the mooring site, close to and consistent with the buoy observations.

The NCEP data come from the recent reanalysis; but, because the recent ECMWF reanalysis was done only up through 1993, ECMWF operational analysis fields were used. Only winds and wind stresses from the FNMOC analysis fields were included, as the air–sea fluxes from this center were not archived, and a reanalysis has not been done. In each comparison, data were obtained from the model grid point nearest to the location of the mooring, every 6 h (ECMWF, NCEP) or 12 h (FNMOC) for a time interval that included the period of the buoy deployment. For ECMWF, the grid point was 15.14°N, 61.875°E, 56.7 km from the buoy; for NCEP, the grid point was 16.19°N, 61.875°E, 86.6 km from the buoy; and for FNMOC model the grid point was 15.5°N, 61.3°E, 21.4 km from the buoy. For the comparisons, the buoy winds were extrapolated to 10 m and the air temperatures and humidities to 2 m to match the models. This was done using boundary-layer profiles computed using the Fairall et al. (1996a) bulk flux algorithm. Monthly means were computed from the numerical weather prediction data and, in addition, the 6- and 12-hourly model data were compared with buoy data subsampled every 6 and 12 h.

Figs. 7 and 8 show overplots of the differences between monthly means of these data sets and the buoy time series from October 1994 through October 1995. Tables 8 and 9 provide a quantitative summary of the annual means and averages over each of the monsoons. The model and observed wind speeds are close, within approximately 0.5 m s^{-1}, during the Northeast Monsoon. The ECMWF wind speeds are close to the buoy winds during both the monsoons but show differences during the intermonsoons. During the Southwest Monsoon, the NCEP and FNMOC winds are 1–2 m s^{-1} lower than observed. The SOC 1994–1995 winds are stronger than all others during the height of the Southwest Monsoon. NCEP wind stress is closest to that observed in the Northeast Monsoon, but all three models underestimate the wind stress during the first two months of the Southwest Monsoon, with ECMWF coming closest to the buoy stresses. Barometric pressure agrees well among the buoy, SOC 1994–1995, and the models; the standard deviation of the monthly differences of each from their mean for that month is 0.63 mb. The NCEP air temperature is low compared to the observed, SOC 1994–1995, and ECMWF air temperatures from October 1994 through May 1995, and the bias is largest, approximately 1°C, in December, January, and February. The model monthly mean sea surface temperatures are close to those

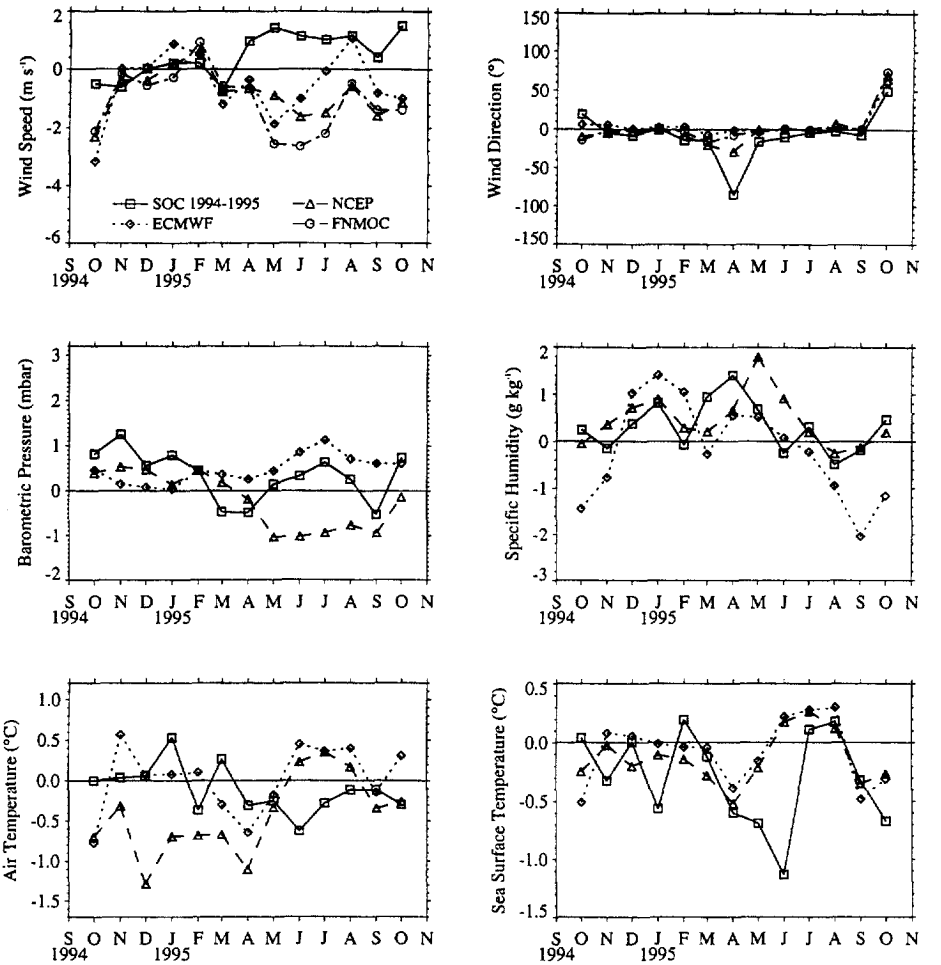

Fig. 7. Overplots of the differences between monthly means of the buoy observations and the FNMOC (wind speed only), ECMWF, and NCEP models, and SOC 1994–1995. The difference is computed as (model–buoy value). Different symbols and line types are used as indicated in the overplot of the wind speeds.

observed at the buoy. ECMWF, for example, which uses the Reynolds sea surface temperature field (Reynolds and Smith, 1994, 1995), shows a mean offset from the buoy of $-0.05°C$. The SOC 1994–1995 and model monthly mean specific humidities are higher than those observed during the Northeast Monsoon by nearly $1\,g\,kg^{-1}$, and ECMWF humidities are drier than those of the buoy and NCEP in September and October by about the same amount.

Both the NCEP and ECMWF monthly net heat flux values are biased low compared to the buoy and SOC 1994–1995 net heat fluxes (Fig. 8). For NCEP this

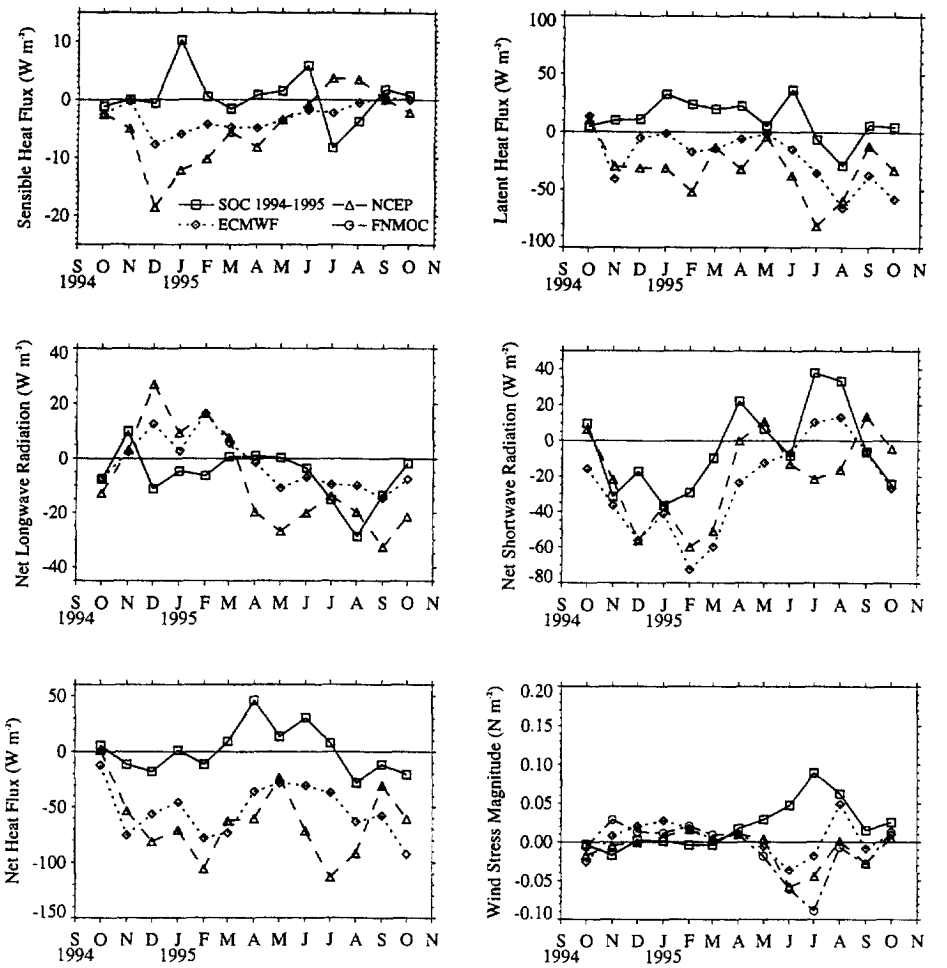

Fig. 8. Overplots of the differences between monthly mean fluxes at the buoy and FNMOC (wind stress only), ECMWF, and NCEP models, and SOC 1994–1995. The difference is computed as (model–buoy value). Different symbols and line types are used as indicated in the overplot of the sensible heat fluxes.

bias is typically 50–100 $W m^{-2}$, and during the two monsoons (Table 9) NCEP net heat fluxes are 70–85 $W m^{-2}$ below that observed. During the Southwest Monsoon, the mean June and July NCEP net heat flux indicates oceanic heat loss, but the buoy monthly mean net heat flux, while reduced, still indicate ocean heating. During the Southwest Monsoon the ECMWF net heat flux is on average 45 $W m^{-2}$ lower than the buoy, but monthly means remain positive. The differences between the buoy and the two model net heat fluxes are noticeably greater than those between the buoy and

Table 8
Annual means of the surface meteorology and air–sea fluxes from the buoy, the ECMWF, NCEP, and FNMOC models for October 1994 through October 1995 and from the 1994–1995 SOC

	Buoy	ECMWF	NCEP	FNMOC	SOC 1994–1995
U_{10m}	7.12	7.34	6.84	6.54	7.6
WD	157	177	157	172	164
AT_{2m}	26.67	26.73	26.25		26.6[a]
SST	27.24	27.20	27.13		26.9
RH_{2m}	78.0	77.5	82.1		79.8[a]
SH_{2m}	16.95	16.86	17.43		17.2[a]
BP	1010.4	1010.9	1010.2		1010.8
P	0.0053		0.0137		0.0053
$\|\tau\|$	0.1007	0.1049	0.0907	0.0900	0.1166
Q_{sen}	−1.7	−4.6	−6.5		−1.2
Q_{lat}	−122.6	−144.1	−154.6		−112.7
SW_{net}	243.3	219.0	222.3		241.1
LW_{net}	−58.7	−60.9	−65.9		−66.0
Q_{net}	60.3	9.4	−4.5		61.3
E-P	0.1747		0.2131		0.1600

[a] SOC 1994–1995 air temperature, relative humidity and specific humidity are 10 m stability dependent values.

the SOC 1994–1995 fields for the same period, the latter typically agreeing to within 20–30 $W m^{-2}$ at month-long time scales.

In terms of the annual mean net heat flux, the buoy and SOC 1994–1995 analyses differ by just 1 $W m^{-2}$, with values of 60.3 and 61.3 $W m^{-2}$, respectively. In contrast, the corresponding values of annual mean net heat flux from ECMWF and NCEP are 9.4 and −4.5 $W m^{-2}$, respectively. In the mean, the ECMWF model gives a windier, drier, warmer atmosphere, with larger sensible, latent, and longwave heat losses from the ocean than observed. The ECMWF model indicates an annual net heat gain by the ocean of 9.4 $W m^{-2}$, over 50 $W m^{-2}$ less heat gain than observed at the buoy. Roughly half the difference comes from the larger latent heat loss in the model and half from reduced incoming shortwave radiation. The NCEP model gives an atmosphere that is 0.4°C cooler and 0.5 $g kg^{-1}$ moister. It indicates an oceanic heat loss for the year, with annual mean net heat flux equal to −4.5 $W m^{-2}$, over 60 $W m^{-2}$ below that from the buoy. The NCEP annual latent heat flux is 30 $W m^{-2}$ more negative; its annual mean net incoming shortwave radiation is 21 $W m^{-2}$ less; and its net longwave radiative heat loss is 7 $W m^{-2}$ more negative than observed.

The comparison of the monthly means shows seasonal variability in the differences between the models and the buoy, indicating relatively persistent departures in the model fields from the observed meteorology and fluxes. However, the difference time series also have considerable variability within each month. The 6- (NCEP, ECMWF) or 12-hourly (FNMOC) values from the numerical weather prediction models were compared to 6- or 12-hourly, sub-sampled values from the mooring data using scatter

Table 9
Means of the surface meteorology and air–sea fluxes from the buoy, ECMWF, NCEP, and FNMOC for the Northeast Monsoon (November 1, 1994–February 15, 1995) and Southwest Monsoon (June 1–September 15, 1995). SOC 1994–1995 means for November, December and January (Northeast monsoon) and June, July and August (Southwest monsoon) are also included

	Buoy		ECMWF		NCEP		FNMOC		SOC 1994–1995	
	NE	SW	NE	SW	NE	SW	NE	SW	NE	SW
U_{10m}	6.62	11.20	7.25	11.32	6.69	10.02	6.61	9.61	6.8	12.7
WD	228	57	231	59	224	60	227	60	225	51
AT_{2m}	25.45	27.54	25.71	27.88	24.72	27.73			25.9[a]	27.4[a]
SST	26.21	27.34	26.25	27.52	26.11	27.47			26.1	27.2
RH_{2m}	71.5	86.1	74.1	81.5	78.3	85.8			72.5[a]	86.8[a]
SH_{2m}	14.37	19.62	15.00	19.00	15.02	19.82			14.9[a]	19.6[a]
BP	1014.8	1005.2	1014.9	1006.0	1015.2	1004.2			1015.6	1005.0
P	0.0030	0.0012			0.0114	0.0153			0.0083	0.0093
$\|\tau\|$	0.0693	0.2221	0.0876	0.2209	0.0701	0.1892	0.0862	0.1720	0.0675	0.3007
Q_{sen}	−4.7	5.3	−9.0	4.0	−16.2	7.4			−1.2	4.0
Q_{lat}	−161.3	−110.0	−176.0	−151.4	−193.2	−165.0			−150.2	−115.6
SW_{net}	221.8	220.2	173.8	225.7	181.4	206.8			188.3	240.3
LW_{net}	−75.4	−26.0	−67.8	−35.7	−62.0	−45.5			−76.2	−41.4
Q_{net}	−19.7	89.5	−79.0	42.6	−90.2	3.7			−39.4	87.3
E-P	0.2337	0.1603			0.2721	0.2268			0.2122	0.1603

[a] SOC 1994–1995 air temperature, relative humidity and specific humidity are 10 m stability dependent values.

plots and simple statistics (Baumgartner et al., 1997). Relative humidity comparisons show large scatter, particularly so for ECMWF. This scatter is reduced in specific humidity for NCEP but less so for ECMWF. Net longwave radiation, latent heat flux, sensible heat flux, and net shortwave radiation also show considerable scatter in both NCEP and ECMWF.

Regressions between the buoy and model data were computed to quantify the performance of the models at replicating the buoy time series. Means and standard deviations of the model-buoy differences, correlation coefficients and two simple linear regressions between the buoy and model data over the entire deployment are summarized in Table 10. The means of the 6- or 12-hourly differences are consistent with the results of the comparison of the monthly values. Low correlation coefficients are associated with the variables noted above that showed the most scatter. In particular, the ECMWF and NCEP relative humidities and net longwave time series do poorly at replicating the observed variability. The two models however do not always perform equivalently. The coefficient, c_1, of the linear regression differs from unity by more than 10% for both models for wind speed, relative humidity, net longwave, and wind stress. However, for NCEP alone such differences are seen for sensible heat flux, air temperature, and barometric pressure, and for ECMWF alone such differences are seen for sea surface temperature, specific humidity, and latent heat flux.

In the 6- and 12-hourly time series, differences are noted both in association with transient events, lasting for one day to one week, and from persistent biases. Fig. 9 shows an overplot of buoy and model meteorological variables from two one-month periods, one from the Northeast Monsoon and one from the Southwest Monsoon. Figs. 10 and 11 overplot the wind stress magnitudes, heat fluxes, and freshwater fluxes for the same two periods.

During the Northeast Monsoon, both NCEP and ECMWF air temperature have periods of several days when they are low relative to the buoy, but these episodes are more frequent and last longer in the NCEP model. In contrast, during the Northeast Monsoon, while both NCEP and ECMWF are more moist, it is the ECMWF model humidities that show the more extreme departures from the observations. The air temperature variability of the models relative to the buoy leads to several-day periods of larger sensible heat loss. NCEP net longwave loss varies in an almost binary manner between close agreement to the buoy and a value that is approximately 40 $W m^{-2}$ smaller; the ECMWF net longwave loss dips only briefly to the smaller value. For the Northeast Monsoon the large negative bias in model net heat flux stems largely from a persistent underestimation in the models of incoming shortwave radiation (overestimation of cloud cover).

During the Southwest Monsoon (Figs. 9–11) the model sea surface and air temperatures show a tendency to be persistently too warm, and the ECMWF humidities to be too dry. Short-lived departures in wind speed from that at the buoy are seen in the ECMWF and FNMOC models. The too-warm sea-surface temperatures elevate the surface saturation specific humidity; as a result, the models show evaporation and latent heat loss elevated relative to those at the buoy. The NCEP net longwave radiation again shows a binary character, either close to that at the buoy

Table 10
Statistics and regressions based on comparisons of the 6-hourly buoy observations and ECMWF, NCEP, and FNMOC data: the mean difference, the standard deviation of the difference, the correlation coefficient (r), and two regressions. Positive mean differences indicate the model is higher than the buoy

Var	Model	Mean	Std. Dev.	r	Regression[a]		
					c_1	c_0	Slope[b]
U_{10m}	ECMWF	0.249	1.860	0.869	0.8940	1.004	1.006
	NCEP	−0.256	1.632	0.892	0.7543	1.494	0.9216
	FNMOC	−0.608	1.761	0.877	0.7113	1.465	0.8738
WD	ECMWF	2.2	32.9	0.957	1.023	2.8	1.018
	NCEP	−1.9	31.4	0.964	1.058	−0.6	1.060
	FNMOC	1.3	31.0	0.964	1.038	2.0	1.035
AT_{2m}	ECMWF	0.070	0.796	0.895	0.9841	0.493	1.003
	NCEP	−0.414	0.830	0.914	1.123	−3.698	0.9850
SST	ECMWF	−0.051	0.499	0.948	0.8878	3.005	0.9978
	NCEP	−0.124	0.461	0.956	0.9265	1.878	0.9952
RH_{2m}	ECMWF	−0.53	9.21	0.405	0.3905	46.99	0.9860
	NCEP	4.11	7.04	0.591	0.4318	48.42	1.045
SH_{2m}	ECMWF	−0.106	1.672	0.821	0.7342	4.401	0.9864
	NCEP	0.477	1.200	0.914	0.9116	1.976	1.025
BP	ECMWF	0.42	0.64	0.992	0.9271	74.05	1.000
	NCEP	−0.31	1.30	0.976	1.132	−133.88	0.9997
$\|\tau\|$	ECMWF	0.00485	0.04734	0.898	0.8640	0.01856	0.9511
	NCEP	−0.00959	0.04454	0.909	0.7864	0.01197	0.8425
	FNMOC	−0.01165	0.05636	0.867	0.6347	0.02578	0.7526
Q_{sen}	ECMWF	−2.89	6.65	0.728	1.096	−2.72	1.199
	NCEP	−4.74	9.47	0.761	1.588	−3.76	1.730
Q_{lat}	ECMWF	−21.84	48.00	0.660	0.7286	−55.13	1.103
	NCEP	−32.30	46.54	0.736	0.9155	−42.66	1.205
SW_{net}	ECMWF	−25.08	82.58	0.959	0.8829	3.42	0.8887
	NCEP	−21.82	83.72	0.959	0.8642	11.24	0.8834
LW_{net}	ECMWF	−2.06	19.53	0.697	0.6875	−20.39	0.981
	NCEP	−6.88	25.59	0.511	0.5332	−34.26	1.026
Q_{net}	ECMWF	−51.87	90.40	0.952	0.8874	−45.06	0.8575
	NCEP	−65.71	93.45	0.949	0.8711	−57.91	0.8326

[a] Model = $c_1 \cdot$ VAWR + c_0 (linear regression)
[b] Model = Slope · VAWR (linear regression forced through the origin)

or a loss of about 20 $W m^{-2}$ larger. Model latent and longwave heat losses contribute more to the buoy-model differences in this monsoon than during the Northeast Monsoon. The low bias in net shortwave is again seen in NCEP but not in ECMWF.

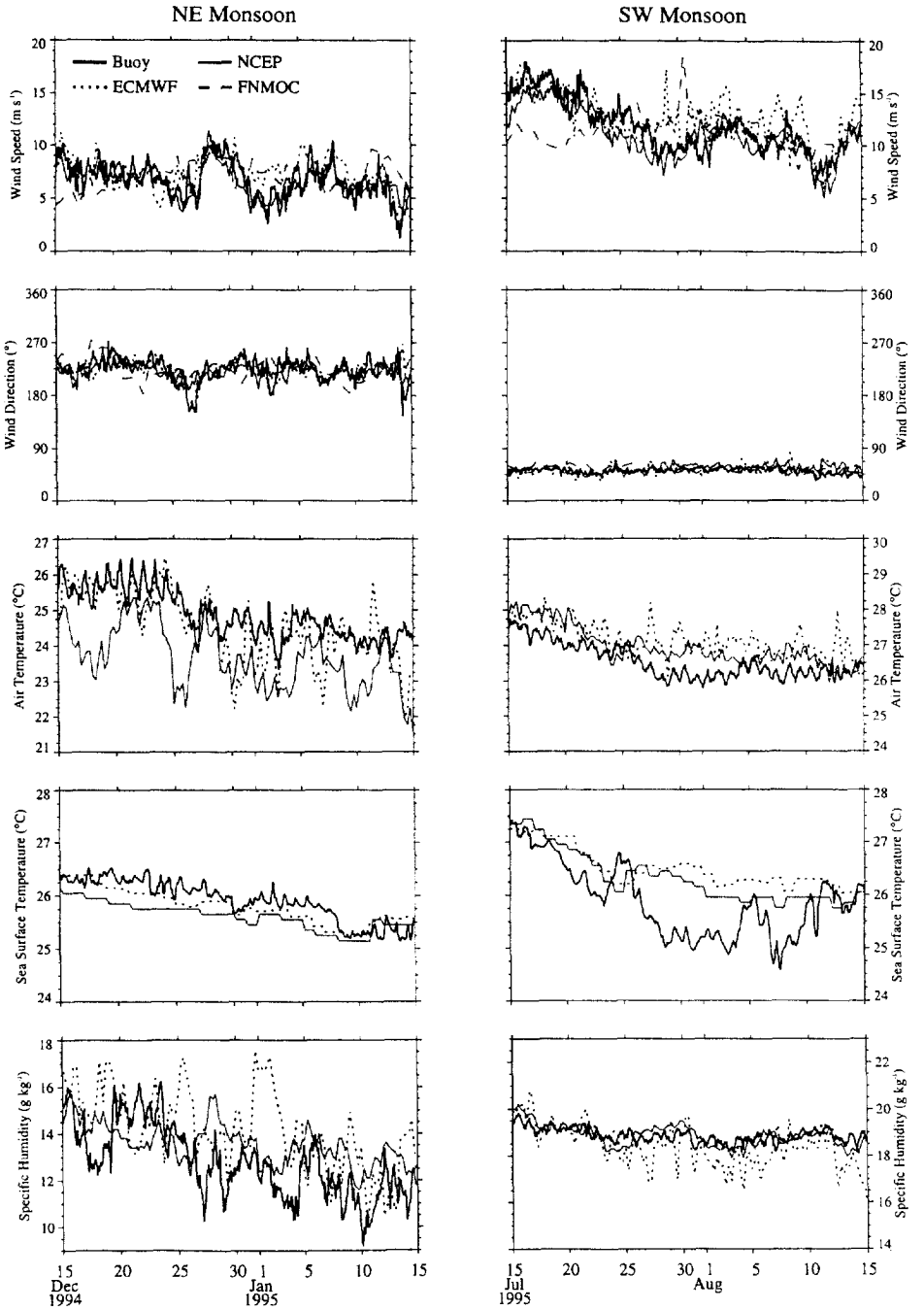
NE Monsoon
SW Monsoon
Buoy
NCEP
ECMWF
FNMOC
Wind Speed (m s⁻¹)
Wind Direction (°)
Air Temperature (°C)
Sea Surface Temperature (°C)
Specific Humidity (g kg⁻¹)
15 Dec 1994
20
25
30
1 Jan 1995
5
10
15
15 Jul 1995
20
25
30
1 Aug
5
10
15

It is interesting to compare Fig. 5 with Fig. 7 and also Fig. 6 with Fig. 8. The model–buoy differences in surface meteorology in Fig. 7 (wind speed and direction, barometric pressure, specific humidity, air temperature, and sea surface temperature) do not track together as closely as do the climatology–buoy differences in Fig. 5. Individual models perform differently at replicating surface meteorology, and these

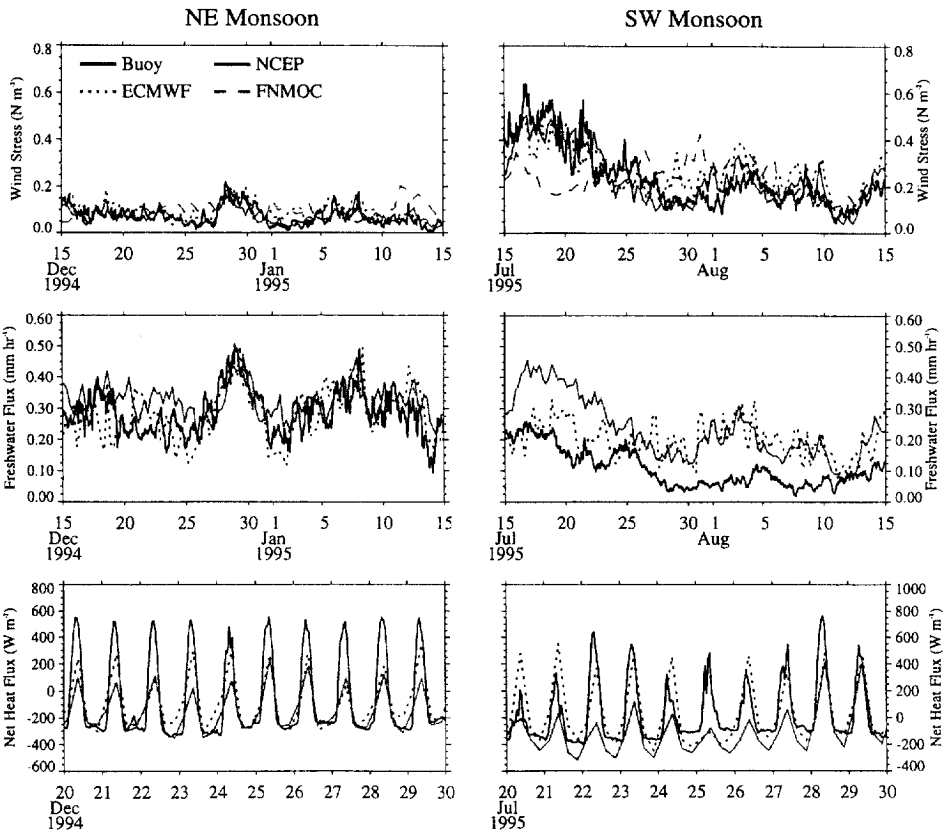

Fig. 10. Overplots (top to bottom) of the wind stress magnitudes, freshwater flux, and net heat flux from one month during the Northeast Monsoon (December 15, 1994–January 15, 1995) (left) and one month during the Southwest Monsoon (July 15–August 15, 1995) (right) from the buoy, FNMOC (wind stress only), ECMWF, and NCEP. Different symbols and line types are used as indicated in the overplot of the wind stress.

Fig. 9. Overplots (top to bottom) of the wind speeds, wind directions, air temperatures, sea temperatures, and specific humidities during one month of the Northeast Monsoon (December 15, 1994–January 15, 1995) (left) and one month during the Southwest Monsoon (July 15–August 15, 1995) (right) from the buoy, FNMOC (wind speed only), ECMWF, and NCEP. Different symbols and line types are used as indicated in the overplot of the wind speeds.

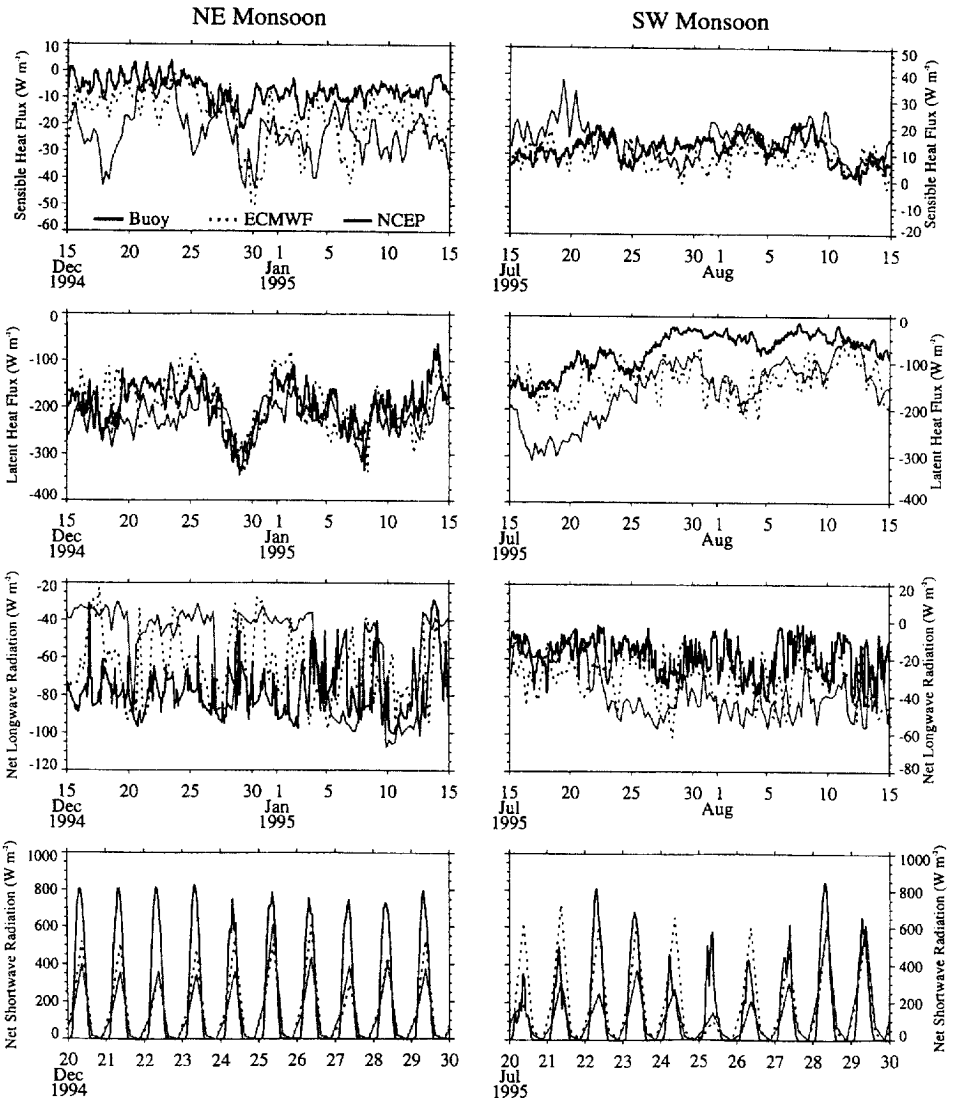

Fig. 11. Overplots (top to bottom) of the sensible heat flux, the latent heat flux, the net longwave heat flux, and the net shortwave heat flux from one month during the Northeast Monsoon (December 15, 1994–January 15, 1995) (left) and one month during the Southwest Monsoon (July 15–August 15, 1995) (right) from the buoy, ECMWF, and NCEP. Different symbols and line types are used as indicated in the overplot of the sensible heat flux.

differences as well as differences in how the models parameterize the flux components contribute to the model–buoy flux differences in Fig. 8. The model-buoy flux differences are as large and sometimes larger than the climatology–buoy flux differences in the corresponding panels in Fig. 6.

5. Was 1994–1995 a typical monsoon year?

The question of whether 1994–1995 was a typical year in terms of the strength of heat exchange and wind stress forcing during the two monsoons can be addressed using the SOC 1980–1995 flux data set. This subset of the individual monthly mean values used to produce the SOC 1980–1995 climatology was extracted for the 1994–1995 period at the location of the buoy and compared against the means over 1980 to 1995. The advantage of using only data from SOC 1980–1995 is that the same method of flux generation has been used throughout, thereby avoiding the problems of different data sources and methods, which hamper any attempt to ascertain whether the deployment period was typical by direct comparison of the buoy observations with the various climatologies.

Time series of the SOC 1994–1995 individual monthly meteorological variables and fluxes are compared with the corresponding climatological values based on the full 1980–1995 data set in Figs. 12 and 13, which include bars showing the interannual standard deviation of the monthly climatological mean. In virtually all cases the meteorological variables and derived fluxes remain within one standard deviation of the climatological means. Looking for the reason why leading the annual mean net heat gain of SOC 1994–1995 is 87.3 $W m^{-2}$ as opposed to the climatological value of 64.0 $W m^{-2}$, there is some indication that the latent heat loss is persistently low throughout the 1995 Southwest Monsoon and the average net shortwave radiation high (Fig. 13; Table 7). However, although larger than the climatological means for June, July, and August, the net heat flux values for these months during 1995 remain within one standard deviation of the climatological means, indicating that this was not an exceptional Southwest Monsoon. The climatological mean net heat flux during the Northeast Monsoon is $-37.3\ W m^{-2}$, and for 1994–1995 the corresponding figure is $-39.4\ W m^{-2}$, suggesting that the Northeast Monsoon sampled by the buoy was close to typical. The wind stress values are close to the climatological mean during each monsoon. Despite large differences between the SOC 1994–1995 precipitation rates and the SOC 1980–1995 climatology, especially during the Southwest Monsoon, the observed rainfall for all months is roughly within one standard deviation of the SOC 1980–1995 climatological means. Since both the 1994–1995 precipitation rates and the latent heat fluxes are close to the SOC climatology, so too is the freshwater flux.

The SOC 1980–1995 and 1994–1995 analyses also were used to consider whether the air–sea fluxes over the Arabian sea as a whole were typical during the deployment period. For the Northeast and Southwest Monsoons, Figs. 14 and 15 show the climatological and 1994–1995 monsoon fields of net heat flux and wind stress over the North Indian Ocean. The climatological and 1994–1995 fields are broadly similar in each case, indicating that the deployment period was not atypical. There is some indication that the region of strongest heat loss over the Arabian Sea during the 1994 Northeast Monsoon has been displaced to the southwest and strengthened. Regarding the 1995 Southwest Monsoon, there appears to be a strengthening of the northwest–southeast gradient in heating across the basin, with the heat loss at the location of the buoy being strengthened in accordance with the comments made above, but

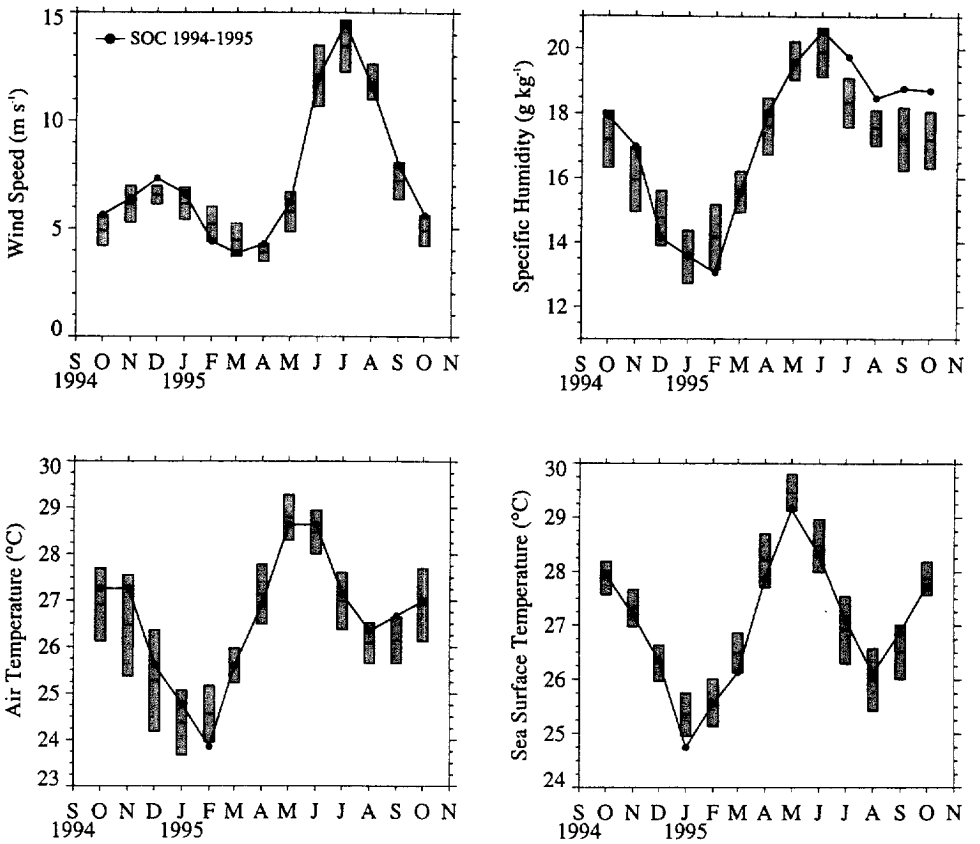

Fig. 12. Overplot of the SOC 1994–1995 monthly mean surface meteorological observables from a 5° × 5° square centered on the buoy location and the SOC 1980–1995 climatological monthly means (horizontal bars in center of gray boxes). The tops and bottoms of the boxes give the interannual standard deviation for the SOC 1980–1995 monthly climatology.

again the field is close to the climatological mean. Finally, the climatological and 1994–1995 wind stress fields are very similar for each monsoon.

In contrast to the monthly statistics, though, comparison of the buoy and FNMOC winds sampled every 12 h suggests some difference between 1994–1995 and the years before and after the experiment. Fig. 16 shows a composite of time series for the 10 m FNMOC winds averaged over three areas encompassing the central and northern Arabian Sea: a southern region (7–12°N, 55–65°E), a central region (10–15°N, 55–65°E), and a northern, coastal region (15–20°N, 55–65°E). To examine interannual variations, the time series for three different one-year periods, October 1993 to October 1996, are overplotted. For all three regions, the wind magnitudes during the buoy deployment are generally consistent with those prior to and following the deployment. This is in agreement with the analysis of the monthly means of SOC

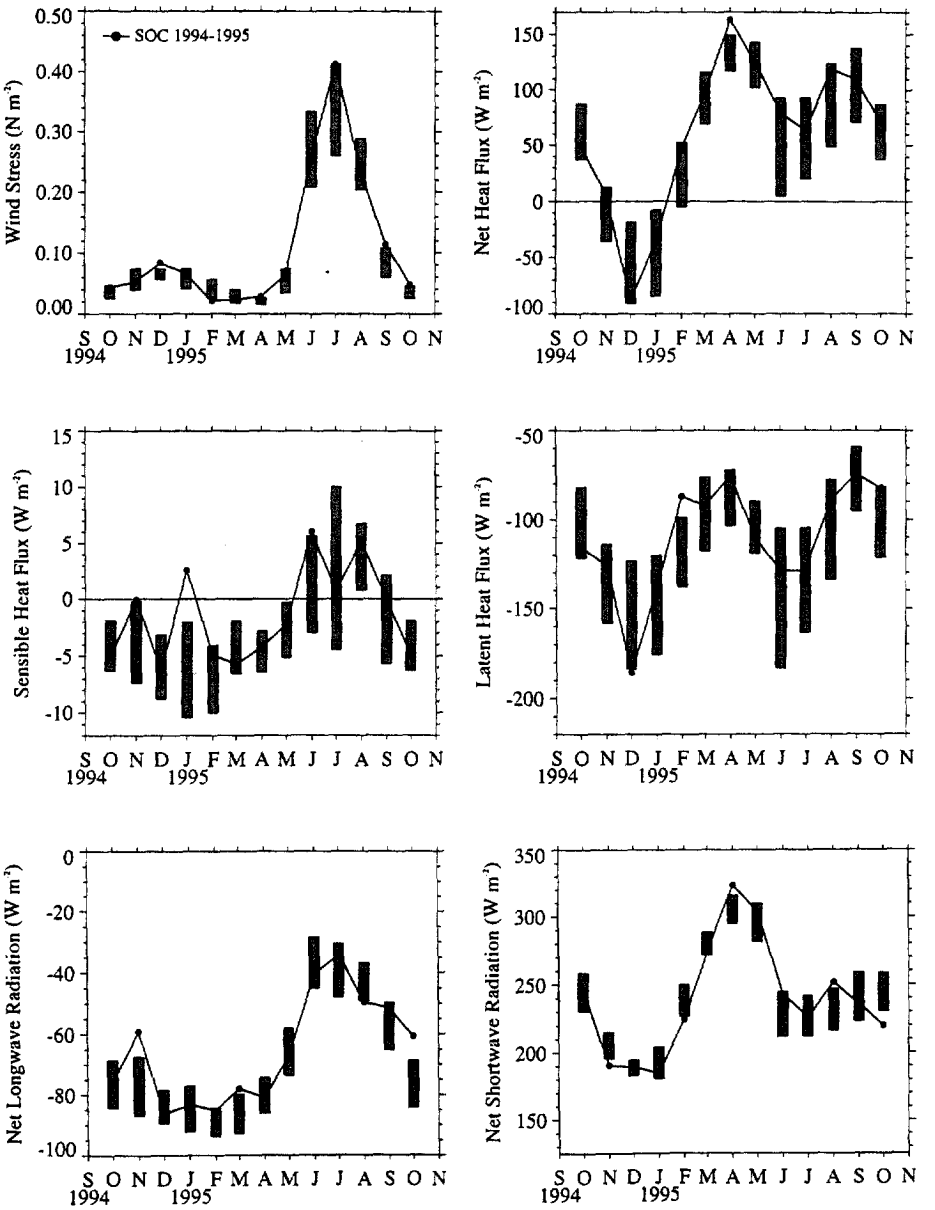

Fig. 13. Overplot of the SOC 1994–1995 monthly mean wind stress, net heat flux, and heat flux components from a 5° × 5° square centered on the location of the buoy and the SOC 1980–1995 climatological monthly means (horizontal bars in the center of the gray boxes). The tops and bottoms of the boxes give the interannual standard deviation for the SOC 1980–1995 monthly climatology.

1994–1995. However, on shorter time scales the intensification of the Southwest Monsoon in the southern and central regions occurred approximately 7–10 days later in 1994–1995 than in the year before and the year after. In addition, in the northern region, in close agreement with the buoy observations, the FNMOC model shows a multiple onset in 1995. Fieux and Stommel (1977) report multiple onsets in only four of the twenty-five years they examined, and the FNMOC winds in the northern region in 1993–1994 and 1995–1996 do not show a multiple onset. Thus, when the variability within one month is examined, the timing and character of the onset of the Southwest Monsoon in 1994–1995 is different from other years.

6. Discussion and summary

The comparisons of the observed meteorology and air–sea fluxes observed at the buoy from October 1994 to October 1995 with both climatological data and meteorology and fluxes from numerical weather prediction models have shown differences. For the comparison between the buoy and the climatologies differences might arise from: (1) measurement error, either at the buoy or in the ship reports, (2) differences in the parameterizations used to calculate the fluxes, (3) the deployment period not being typical, and (4) differences in how the area near the buoy was sampled.

We believe that the uncertainties in the buoy data and derived fluxes are well known based on the extensive investigation of the methodology in TOGA COARE, and that the major differences we find are large compared to the measurement errors in Table 2. The SOC 1980–1995 climatology results from an effort to reduce the uncertainties due to the measurement error in the ship reports on which it, like the other climatologies, is based and to make regionally appropriate choices of the bulk formulae. The good agreement between SOC 1994–1995 and the buoy suggests that the corrections made in the SOC 1980–1995 analyses have improved the accuracy of flux fields derived from ship observations.

Further, the comparison of the SOC 1994–1995 data with the SOC means for 1980–1995 shows that 1994–1995 was in many ways a typical year; 1994–1995 monthly values were almost always within one standard deviation of the 1980–1995 mean values. Only by looking at variability on time scales of days to one week do we find evidence that 1994–1995 may not be typical.

Sampling issues include consideration of the density and location of ship reports in space and time relative to the location of the buoy. The buoy site is in a region characterized by significant space and time gradients, and there is the potential that a skewed distribution of points might result in a bias relative to the buoy reports. Monthly means based on both $1^\circ \times 1^\circ$ and $5^\circ \times 5^\circ$ squares were computed for SOC 1994–1995 and little difference found, suggesting that this is not a problem. As all the climatologies use basically the same ship reports, they should all be similarly affected by sampling error.

Similar issues must be considered for the comparison of the buoy observations and the model fields, where the nearest grid points were chosen for the comparison. For the major differences, the product of the spatial separation times the spatial gradients

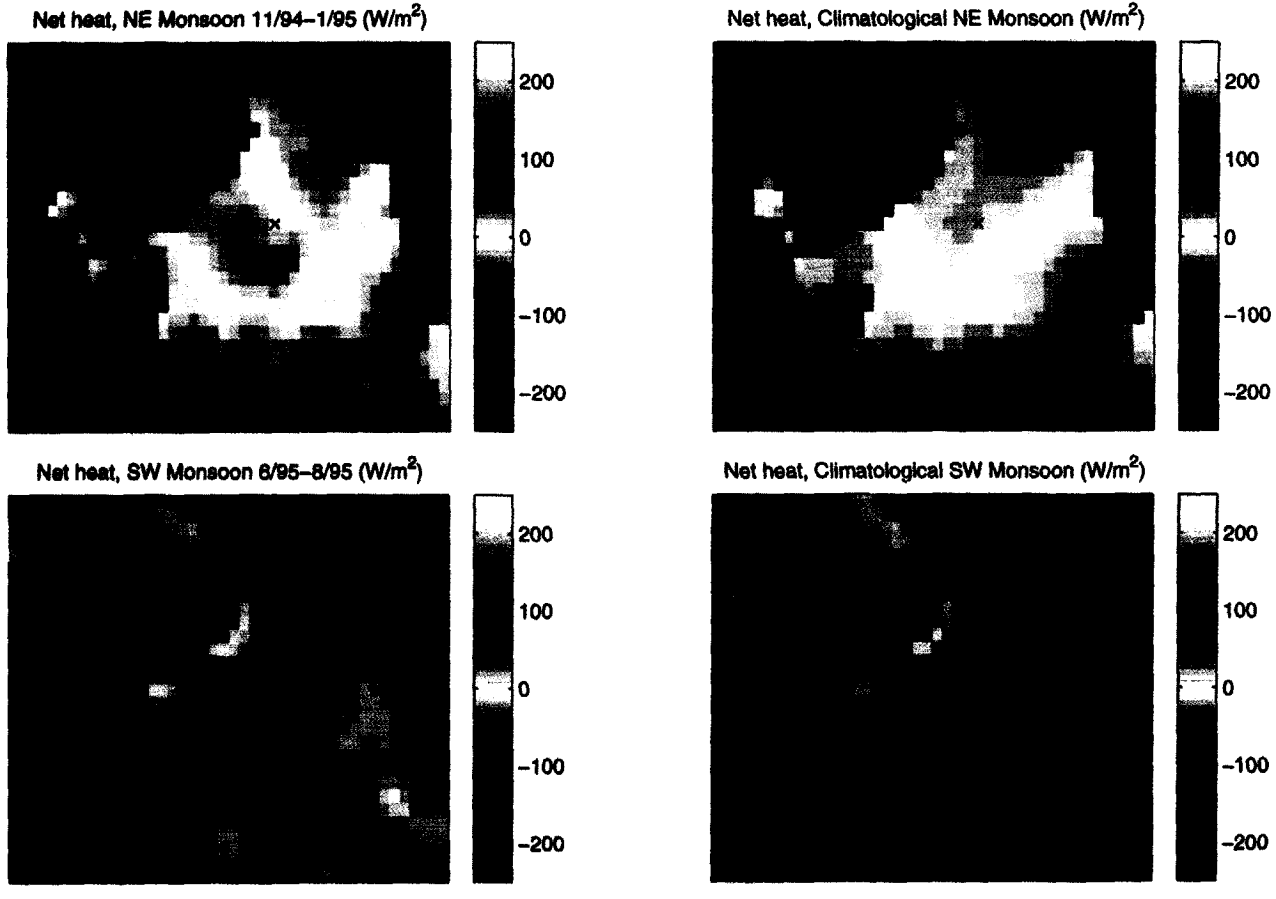

Fig. 14. Maps of the net heat flux over the Arabian Sea from the SOC for the Northeast Monsoon (top) and Southwest Monsoon (bottom). The maps on the left are for 1994–1995; those on the right are the mean of the SOC for 1980-1995. The location of the mooring is marked by an x.

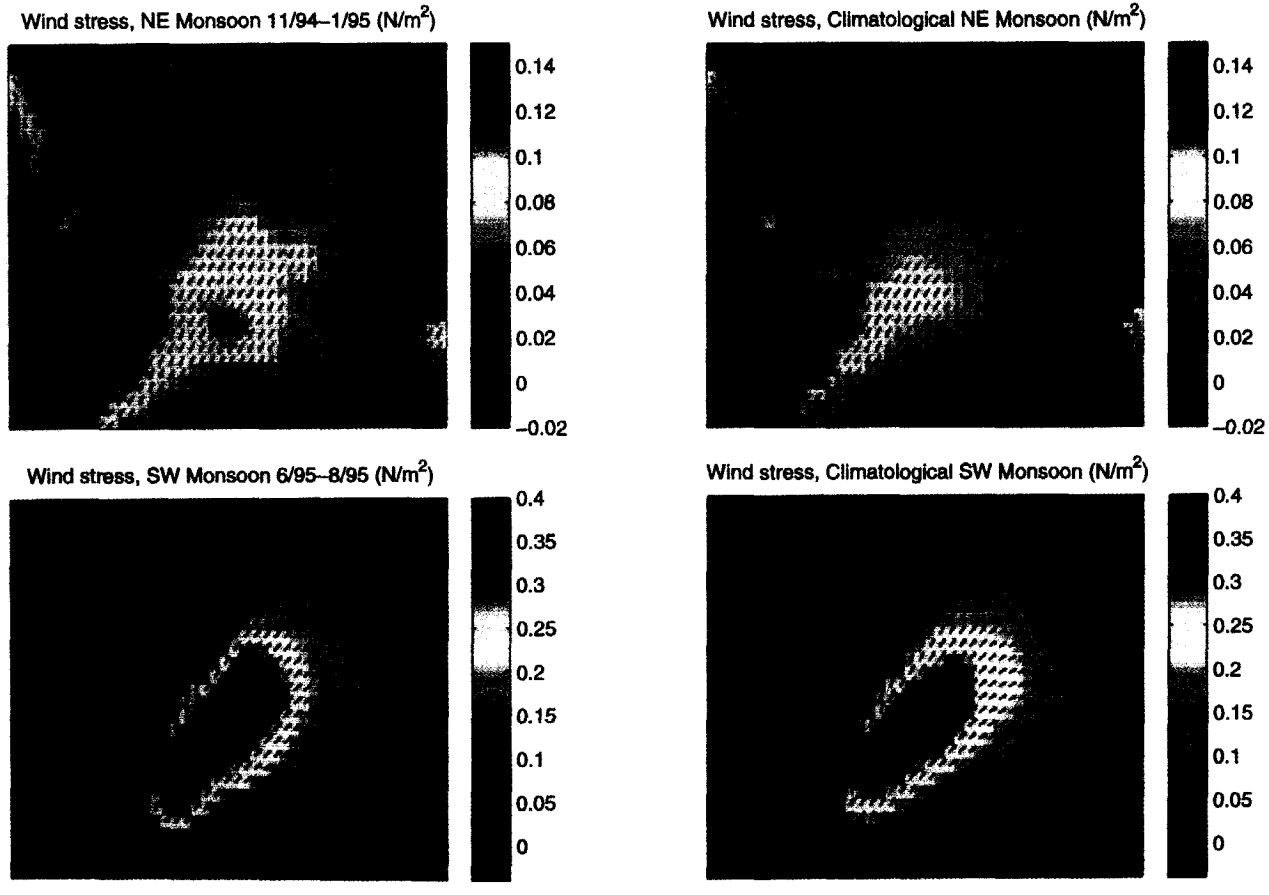

Fig. 15. Maps of the wind stress over the Arabian Sea from the SOC for the Northeast Monsoon (top) and Southwest Monsoon (bottom). The maps on the left are for 1994–1995; those on the right are the mean of the SOC for 1980–1995. The location of the mooring is marked by an x.

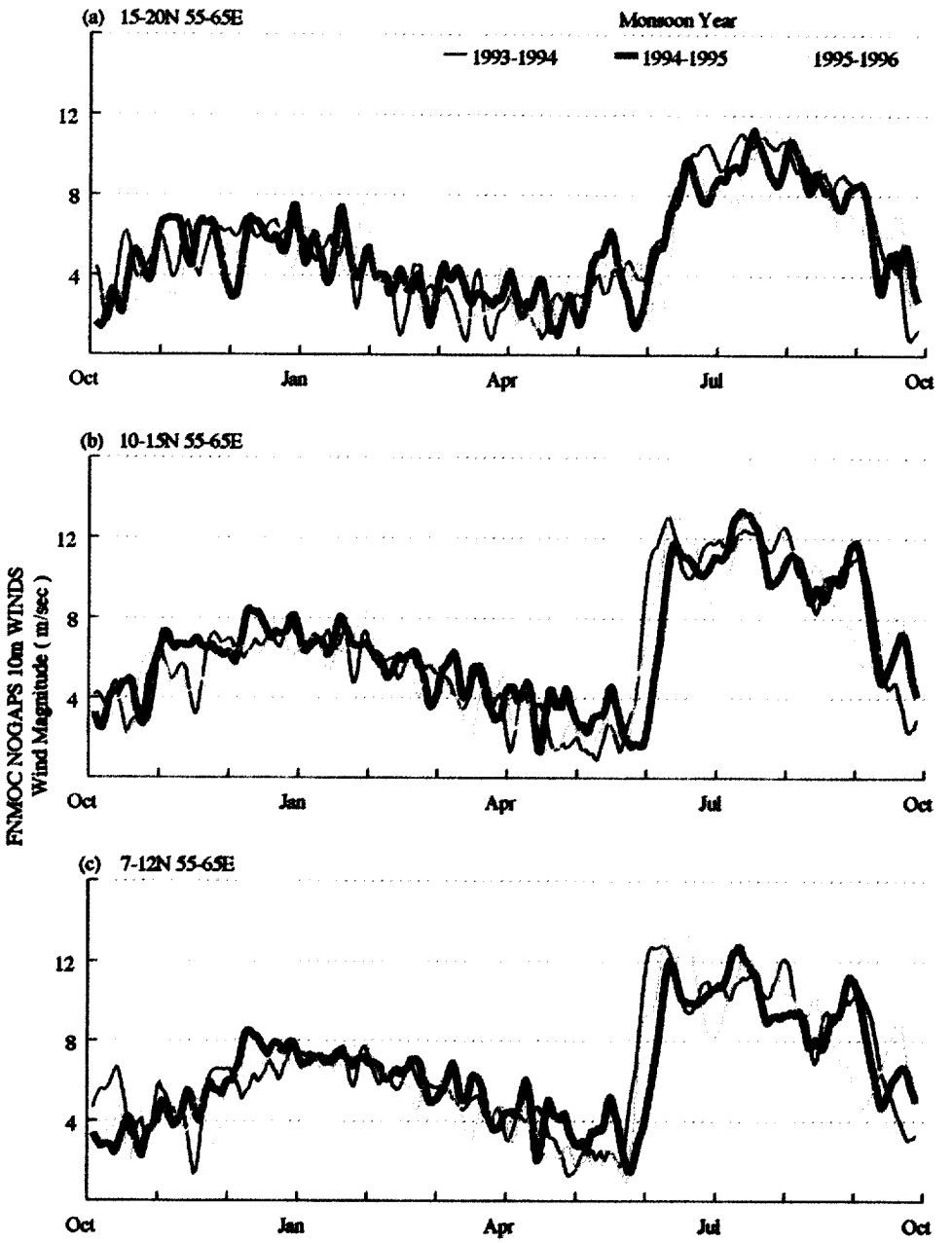

Fig. 16. Overplots of the wind speeds for three different years from the FNMOC model averaged in three geographic regions in the Arabian Sea. The 12-hourly time series are filtered with a 5-day moving average.

observed in the model was most often small compared to the observed differences. Exceptions to this were seen in the ECMWF model, where large spatial gradients were found in relative humidity as regions of greatly different relative humidity migrated around the basin. For net shortwave the 6-hourly accumulations available from the models lead to differences with the buoy, but these are small compared to the differences in mean net shortwave seen, for example, during the Northeast Monsoon. Thus, the differences found between the models and the buoy, particularly in air temperature, humidity, shortwave radiation, cloud cover, and longwave radiation, are taken to primarily reflect the difficulty those models have in producing realistic surface meteorology and air–sea fluxes in the Arabian Sea. In part this is because their sea surface temperatures, which are supplied externally, are at times different from those observed, which affects the boundary layer profiles of temperature and humidity.

Thus, we believe that the differences we find are significant and that there should be concern about the use of climatological or model-based fluxes to investigate air-sea interaction and the physical and biological response of the upper ocean in the Arabian Sea. The Hastenrath, Oberhuber, and Hellerman climatologies do poorly at representing the insolation, net heat flux, and wind stress there. Use of the NCEP net heat flux during the Southwest Monsoon, which indicates a net oceanic heat loss in June and July, would, like the Hastenrath and Oberhuber climatologies, lend support to the conclusion that surface heat loss was important to the mixed layer deepening observed during the summer monsoon. Instead, using the buoy data, in which the June and July monthly net oceanic heat gains were 48.7 and 56.0 $W m^{-2}$, Fischer (1997) concludes that wind-driven shear rather than convection drives the mixing. SOC 1994–1995 and SOC 1980–1995, like the buoy, indicate that the Southwest Monsoon is associated with heat gains of greater than 60 $W m^{-2}$. With such strong surface heating, closure of the local upper ocean heat budget requires another process, perhaps the inflow of cool water upwelled along the coast.

Posing the possibility that the biases between the observed, climatological and model fluxes may be found over the whole Arabian Sea, we considered the significance of these differences. To set the context, note that Wacogne and Pacanowski (1996) describe a meridional circulation in the Indian Ocean that moves 1×10^{15} W of heat northward across the equator in the Northeast Monsoon (February) and 1.2×10^{15} W of heat southward in the Southwest Monsoon (August). The annual biases in the net heat flux, -50.9 and -64.8 $W m^{-2}$ relative to the buoy, respectively, for ECMWF and NCEP if uniform over the basin (an area of 6.4×10^{12} m^2). Düing and Leetmaa (1980) would correspond to a shift in the surface heating in 1994–1995 by $0.3–0.4 \times 10^{15}$ W. The Hastenrath and Oberhuber net heat fluxes show smaller biases; but, if that bias was spatially uniform, it would shift surface heating by $0.1–0.2 \times 10^{15}$ W, the same size as the 0.2×10^{15} W annual mean heating reported for the region by Düing and Leetmaa (1980). If the higher mean heating seen at the buoy and by SOC reflects a bias found over the entire Arabian Sea, the actual 1994–1995 heating would be two to three times higher than that based on older climatologies. This, in turn, would require a stronger oceanic export of heat from the Arabian Sea.

In studies of seasonal variability of the meridional transport of heat out of the northern Indian Ocean (e.g., Lee and Marotzke, 1998) the choice of Hellerman wind

stress would lead to an overestimate of the Ekman transport of warm water southward during the Southwest Monsoon by 45%. ECMWF winds are higher than observed at the buoy site in the annual mean and particularly during the Northeast Monsoon. Halpern et al. (1998) find over the Arabian Sea that use of the ECMWF winds results in meridional Ekman transport at 8.5°N that are 32% larger than those computed using NCEP winds. If a biased low heat flux climatology is used together with wind stresses that are too large, the net surface heat transport might not be unrealistic. Still, simplifications such as taking the net shortwave and longwave radiation each to be constant (Wacogne and Pacanowski, 1996), may be a source of error in such studies. At the buoy, the net longwave radiation varies by 50 $W m^{-2}$ and the shortwave radiation varies by 100 $W m^{-2}$ over the year.

The good agreement between the new SOC 1994–1995 data set and the buoy allow us to use the SOC data from 1980–1995 to establish that the buoy deployment was done in a generally typical year. It also encourages us to choose the SOC 1980–1995 data set to pursue further questions about the heat budget of the Arabian Sea. Flux variability at the mooring site showed that accurate sea-surface temperature, atmospheric moisture content, and insolation data are needed as a basis for determining the fluxes accurately. Particularly during the Southwest Monsoon, the cooling of the sea-surface temperature in combination with the high humidity of the air reduced latent heat loss. The moist atmosphere also reduced outgoing longwave radiation. Accurate determination of the radiative fluxes has long been a challenge in preparing climatologies. The SOC 1980–1995 climatology is an improvement. Numerical weather prediction models still need to make improvements in determining shortwave radiation. They also need to receive good sea surface temperatures and to improve the air temperatures (NCEP) and humidities in order to produce more accurate fluxes.

In summary, the year-long time series from a surface mooring deployed off the coast of Oman along the climatological axis of the Findlater Jet showed strong monsoonal variability. The Northeast Monsoon was characterized by steady but moderate winds, clear skies, relatively dry air, and two months, December and January, in which the ocean, on average, lost 45 $W m^{-2}$ to the atmosphere. The Southwest Monsoon had strong winds, cloudy skies, and moist air and was accompanied by sustained oceanic heat gain, with the strongest monthly mean warming of the year, 147 $W m^{-2}$, in August. Large differences are found between the observations and older air-sea flux climatologies, particularly so in the Southwest Monsoon, when the older climatologies indicate oceanic heat loss. Recent climatologies agree better with the observations. Based on monthly means, comparison of the SOC 1980–1995 and SOC 1994–1995 data sets shows that 1994–1995 was a typical year. At the higher temporal resolution provided by the FNMOC winds, however, the timing and character of the onset of the Southwest Monsoon in 1995 differs from other years. Comparison with concurrent data from NCEP, ECMWF, and FNMOC shows that the models provide realistic surface winds, but fail to replicate other observed surface meteorology and to produce realistic heat fluxes. Annual and monsoonal mean net heat fluxes from the models differ from those of the buoy by 50–80 $W m^{-2}$. Because of these differences, some care is warranted in selecting and using air-sea flux fields in studies of the Arabian Sea.

Acknowledgements

The members of the Woods Hole Oceanographic Institution Upper Ocean Processes Group involved in preparation and deployment of the buoy and in processing the data are thanked, including Rick Trask, Will Ostrom, Bryan Way, Jon Ware, Dick Payne, Dave Hosom, Geoff Allsup, Nancy Brink, and Nan Galbraith. Dr. Steve Anderson's help with understanding the performance of the meteorological sensors and developing methods to reduce their error and Dr. Peter Taylor's helpful comments are gratefully acknowledged. The work at Woods Hole Oceanographic Institution was funded by the Office of Naval Research, Grant N00014-94-1-0161. This is Contribution Number 9569 from the Woods Hole Oceanographic Institution. The analysis of the Southampton Oceanography Centre fields described in this paper was partially funded by a commissioned research project for the Hadley Centre, U.K. Meteorological Office. The Naval Research Laboratory participation was funded through the 6.1 Forced Upper Ocean Dynamics ARI under Program Element 61153N sponsored by the Office of Naval Research. This is U.S. JGOFS contribution number 419.

References

Anderson, S.P., Baumgartner, M.F. 1998. Radiative heating errors in naturally ventilated air temperature measurements made from buoys. Journal of Atmospheric and Oceanic Technology 15, 157–173.

Baumgartner, M.F., Brink, N.J., Ostrom, W.M., Trask, R.P., Weller, R.A., 1997. Arabian Sea Mixed Layer Dynamics Experiment Data Report. Upper Ocean Processes Group Technical Report 97-3, WHOI-97-08, Woods Hole Oceanographic Institution, Woods Hole, MA, USA 02543, 169 pp.

Bignami, F., Marullo, S., Santoleri, R., Schiano, M.E., 1995. Longwave radiation budget in the Mediterranean Sea. Journal of Geophysical Research 100, 2501–2514.

Clark, N.E., Eber, L., Laurs, R.M., Renner, J.A., Saur, J.F.T. 1974. Heat exchange between ocean and atmosphere in the eastern North Pacific for 1961–71. NOAA Techical Report NMFS SSRF-682, U. S. Dept. of Commerce, Washington, DC, 72 pp.

Da Silva, A.M., Young, C.C., Levitus, S. 1994. Atlas of surface marine data 1994. Volume 1: Algorithms and procedures. NOAA Atlas NESDIS 6, U. S. Dept. of Commerce, Washington, DC, 83 pp.

Düing, W., Leetmaa, A. 1980. Arabian sea cooling: a preliminary heat budget. Journal of Physical Oceanography 10, 307–312.

Fairall, C.W., Bradley, E.F., Rogers, D.P., Edson, J.B., Young, G.S., 1996a. Bulk parameterization of air–sea fluxes for TOGA COARE. Journal of Geophysical Research 101, 3747–3764.

Fairall, C.W., Bradley, E.F., Godfrey, J.S., Wick, G.A., Edson, J.B., Young, G.S. 1996b. Cool-skin and warm-layer effects on sea surface temperature. Journal of Geophysical Research 101, 1295–1308.

Fieux, M., Stommel, H. 1977. Onset of the Southwest Monsoon over the Arabian Sea from marine reports of surface winds. Monthly Weather Review 105, 231–236.

Fischer, A.S., 1997. Arabian Sea mixed layer deepening during the monsoon: observations and dynamics. M. S. Thesis, Massachusetts Institute of Technology and Woods Hole Oceanographic Institution, Woods Hole, Massachusetts, 130 pp.

Gill, G.C., 1983. Comparison testing of selected naturally ventilated solar radiation shields. Report submitted to NOAA Data Buoy Office, Bay St. Louis, Mississippi In partial fulfillment of Contract #NA-82-01-A-266, September 1983. NOAA/National Data Buoy Center, Bay St. Louis, Mississipi 39529, USA.

Halpern, D., Freilich, M.H., Weller, R.A. 1998. Arabian sea surface winds and ocean transports determined from ERS-1 scatterometer. Journal of Geophysical Research 103, 7799–7806.

Hastenrath, S., Lamb, P.J., 1979a. Climatic Atlas of the Indian Ocean. Part 2: The oceanic heat budget. University of Wisconsin Press, Madison, Wisconsin, 110 pp.

Hastenrath, S., Lamb, P., 1979b. Climatic Atlas of the Indian Ocean. Part 1: Surface circulation and climate. The University of Wisconsin Press, Madison, Wisconsin, 116 pp.

Hellerman, S., Rosenstein, M., 1983. Normal monthly wind stress over the world ocean with error estimates. Journal of Physical Oceanography 13, 1093–1104.

Hosom, D.S., Weller, R.A., Payne, R.E., Prada, K.E., 1995. The IMET (Improved Meteorology). Ship and Buoy Systems. Journal of Atmospheric and Oceanic Technology 12, 527–540.

Josey, S.A., Kent, E.C., Oakley, D., Taylor, P.K., 1996. A new global air–sea heat and momentum flux climatology. International WOCE Newsletter 24, 3–5.

Josey, S.A., Oakley, D., Pascal, R.W., 1997. On estimating the atmospheric longwave flux at the ocean surface from ship meteorological reports. Journal of Geophysical Research 102, 27961–27972.

Josey, S.A., Kent, E.C., Taylor, P.K., 1998. Ocean-atmosphere heat exchange: a global climatology derived from in situ meteorological observations. Journal of Climate (in preparation).

Lee, T., Marotzke, J., 1998. Seasonal cycles of meridional overturning and heat transport of the Indian Ocean. Journal of Physical Oceanography, submitted.

List, R.J., 1984. Smithsonian Meteorological Tables. Smithsonian Institution Press, Washington DC, 527 pp.

Oberhuber, J.M., 1988. An atlas based on the COADS data set: the budgets of heat, buoyancy and turbulent kinetic energy at the surface of the global ocean. Max-Planck-Institute for Meteorology Report No. 15, Max-Planck-Institüt fur Meteorologie, 2000 Hamburg 13, Bundestrass 55, FRG. 20 pp. 247 Figs.

Ostrom, W.M., Way, B.S., Weller, R.A., Ware, J.D., Trask, R.A., 1996. Arabian Sea Mixed Layer Dynamics Experiment: Mooring Cruise Report R/V Thomas Thompson Cruise Number 52 14 October–25 October 1995. Upper Ocean Processes Group Technical Report 96-2, WHOI-96-11, Woods Hole Oceanographic Institution, Woods Hole, Masachusetts 02543, USA, 72 pp.

Payne, R.E., 1972. Albedo of the sea surface. Journal of Atmospheric Sciences 29, 959–970.

Payne, R.E., 1987. Air temperature shield tests. Woods Hole Oceanographic Institution Technical Report No.WHOI 87-40, Woods Hole, Massachusetts 02543, USA, 22 pp.

Reynolds, R.W., Smith, T.M., 1994. Improved global sea surface temperature analyses. Journal of Climate 7, 929–948.

Reynolds, R.W., Smith, T.M., 1995. A high resolution global sea surface temperature climatology. Journal of Climate 8, 1572–1583.

Smith, S.D., 1980. Wind stress and heat flux over the ocean in gale force winds. Journal of Physical Oceanography 10, 709–726.

Trask, R.P., Way, B.S., Ostrom, W.M., Allsup, G.P., Weller, R.A., 1995a. Arabian Sea Mixed Layer Dynamics Experiment: Mooring Cruise Report R/V Thomas Thompson Cruise Number 40, 11–25 October 1994. Upper Ocean Processes Group Technical Report 95-1, WHOI-95-01, Woods Hole Oceanographic Institution, Woods Hole, MA USA 02543, 64 pp.

Trask, R.P., Weller, R.A., Ostrom, W.M., 1995b. Arabian Sea Mixed Layer Dynamics Experiment: Mooring Cruise Report R/VThomas Thompson Cruise Number 46, 14–29 April 1995. Upper Ocean Processes Group Technical Report 95-14, WHOI-95-04, Woods Hole Oceanographic Institution, Woods Hole, Masachusetts 02543, USA, 92 pp.

Trask, R.P., Weller, R.A., 1995. Cyclic fatigue testing of surface mooring hardware for the Arabian Sea Mixed Layer Dynamics Experiment. Upper Ocean Processes Group Technical Report 95-5, WHOI-95-16, Woods Hole Oceanographic Institution, Woods Hole, Massachusetts 02543, USA, 63 pp.

Wacogne, S., Pacanowski, R., 1996. Seasonal heat transport in a primitive equations model of the tropical Indian Ocean. Journal of Physical Oceanography 26, 2666–2699.

Weller, R.A., Rudnick, D.L., Payne, R.E., Dean, J.P., Pennington, N.J., Trask, R.P., 1990. Measuring near-surface meteorology over the ocean from an array of surface moorings in the subtropical convergence zone. Journal of Atmospheric and Oceanic Technology 70, 85–103.

Weller, R.A., Anderson, S.P., 1996. Surface meteorology and air–sea fluxes in the western equatorial Pacific warm pool during the TOGA Coupled Ocean–Atmosphere Response Experiment. Journal of Climate 9, 1959–1990.

Wright, P.B., 1988. An atlas based on the "COADS" data set: fields of mean wind, cloudiness, and humidity at the surface of the global ocean. Max-Planck-Institute for Meteorology Report No. 14, Max-Planck Institüt fur Meteorologie, 2000 Hamburg 13, Bundestrass 55, FRG, 7 pp., 60 fig.